Geologic evolution of the Martian dichotomy in the Ismenius area of Mars and implications for plains magnetization

S. E. Smrekar,[1] G. E. McGill,[2] C. A. Raymond,[1] and A. M. Dimitriou[2,3]

Received 5 March 2004; revised 15 June 2004; accepted 19 August 2004; published 13 November 2004.

[1] The origin of the Martian dichotomy, which divides highlands from lowlands, is unknown. We examine a section of the dichotomy (50–90E) defined by steep scarps and normal faults. Stratigraphy and age relationships preclude the formation of the 2.5 km high boundary via erosion. The abrupt disappearance of topographic knobs ~300–500 km to the northeast is interpreted as a buried fault. Alignment of the buried fault with grabens, stratigraphy, and age determinations using crater counts indicate that the lowland bench is down faulted highlands crust. The estimated local strain (3.5%) and fault pattern are broadly consistent with gravitational relaxation of a plateau boundary. Magnetic and gravity anomalies occur on either side of the buried fault. Admittance analysis indicates isostatic compensation. Although nonunique, a model with a 10 km thick intracrustal block under the lowland bench, a 20 km thick block under the plains, and an excess density of 200 kg/m^3 provides a good fit to the isostatic anomaly. A good fit to a profile of the magnetic field perpendicular to the dichotomy is produced using uniformly polarized intracrustal blocks 10–20 km thick, an intensity of 6 Am/m, a field inclination of −30°, and gaps aligned with the isostatic anomalies. One interpretation is that high-density intrusions demagnetized the crust after dynamo cessation and that low-lying magnetized areas could be down faulted highlands crust. Another model (inclination of 30°) has magnetized crust beneath the isostatic anomalies, separated by gaps. The gaps could result from hydrothermal alteration of the crust along fault zones. *INDEX TERMS:* 6225 Planetology: Solar System Objects: Mars; 1219 Geodesy and Gravity: Local gravity anomalies and crustal structure; 1517 Geomagnetism and Paleomagnetism: Magnetic anomaly modeling; 5475 Planetology: Solid Surface Planets: Tectonics (8149); 8010 Structural Geology: Fractures and faults; *KEYWORDS:* Mars, dichotomy, crustal magnetism, gravity, isostasy, faulting, gravitational relaxation, extension

Citation: Smrekar, S. E., G. E. McGill, C. A. Raymond, and A. M. Dimitriou (2004), Geologic evolution of the Martian dichotomy in the Ismenius area of Mars and implications for plains magnetization, *J. Geophys. Res.*, *109*, E11002, doi:10.1029/2004JE002260.

1. Introduction

[2] The global dichotomy is a fundamental feature of Mars, and divides the northern lowlands from the southern highlands. The dichotomy boundary encircles the planet at latitudes ranging from just south of the equator to around 50N, except where interrupted by relatively young volcanic provinces, such as the Tharsis rise, and by impact basins such as Isidis. The formation mechanism for the dichotomy is uncertain. A variety of exogenic and endogenic models have been proposed. Exogenic models consist of either a single impact basin termed the Borealis basin [*Wilhelms and Squyres*, 1984], or multiple, overlapping large impact events [*Frey and Schultz*, 1988]. Endogenic models include a primordial crustal thickness variation [*Mutch et al.*, 1976], thinning of the crust and/or lithosphere above a degree 1 mantle convection pattern [*Wise et al.*, 1979a, 1979b; *Breuer et al.*, 1997, 1998; *Zhong and Zuber*, 2001], resurfacing due to plate tectonics [*Sleep*, 1994], and preservation of crustal thickness differences that existed when Mars transitioned from plate tectonics to stagnant lid convection [*Lenardic et al.*, 2004]. Distinguishing between these models would help constrain the overall thermal evolution of the planet, possibly timing of core formation, and the associated mantle heat flux over time. This in turn may constrain of the timing of the demise of the magnetic dynamo and the loss of the early atmosphere, as well as the role of interior heat flux in creating liquid water on the surface of Mars.

[3] The dichotomy boundary consists of an increase in elevation from the northern lowlands to southern highlands of 2–4 km typically, and more than 6 km locally within a transition zone several 100s km to as much as 1300 km wide [*Frey et al.*, 1998; *Smith et al.*, 1999]. Initial estimates from Mars Orbiter Laser Altimeter (MOLA) data indicate that the average slope across the transition zone is about 1° [*Frey et al.*, 1998]. The boundary also represents a change in roughness due to the transition from a heavily cratered region in the south to a relatively smooth, uncratered surface

[1]Jet Propulsion Laboratory, California Institute of Technology, Pasadena, California, USA.
[2]Department of Geosciences, University of Massachusetts, Amherst, Massachusetts, USA.
[3]SLR Alaska, Anchorage, Alaska, USA.

0148-0227/04/2004JE002260$09.00

in the north [*Smith et al.*, 1999]. Where unmodified by younger volcanism, the boundary is transitional or else consists of either a single scarp or a series of eroded fractures [e.g., *McGill and Dimitriou*, 1990]. A key question is how the scarps and steep slopes relate to the formation of the dichotomy and any subsequent modification.

[4] Several lines of evidence indicate that the dichotomy formed early in the history of Mars. Stratigraphy indicates that the dichotomy formed in the Noachian period [*Tanaka et al.*, 1992; *McGill and Dimitriou*, 1990], but whether it formed early or late in the Noachian remains controversial. *Frey* [2004] recently used crater counts of both surficial and buried craters to place the formation of the dichotomy at 4.04 ± 0.08 Ga. Several studies of the gravity and topography indicate that the southern highlands and the dichotomy are isostatically compensated [*Nimmo and Stevenson*, 2001; *McGovern et al.*, 2002; *McKenzie et al.*, 2002; *Nimmo*, 2002], which implies that the boundary formed while thermal gradients remained high. These studies indicate that the dichotomy is preserved from the first 0.5–1 b.y. of Martian history. It is impressive, and puzzling, that areas of such steep topography have been preserved for so long given that they formed during a time when heat flow from the interior was likely to be high. Another challenge for explaining the present topography of the dichotomy is that few of the endogenic models for the origin are likely to result in steep boundaries. The Moon is believed to have differentiated such that the far side has thicker crust than the nearside, but there is no abrupt change in elevation that reflects this asymmetry [*Zuber et al.*, 1994]. Nor do degree one convection models predict any type of steep transition [*Zhong and Zuber*, 2001]. Of all the models of origin, only plate tectonics [*Sleep*, 1994; *Lenardic et al.*, 2004] predicts a steep boundary. However, other factors argue against this idea, as discussed below.

[5] Thus a key question is how did the dichotomy boundary become (and remain) so steep in many areas? Are the steep scarps a result of the formation of the dichotomy or do they represent secondary modification? How has the boundary been modified by tectonics, erosion and deposition? As discussed below, erosion has not been a major factor in forming the steep scarps, although some erosion has certainly occurred since formation. The difference in elevation and crustal thickness across some regions of the boundary indicates that there is a pressure differential that may be capable of driving gravitational relaxation and lower crustal flow for sufficiently weak rheologies. Gravitational relaxation would reduce plateau elevations and slopes. Modeling the evolution of the topography at the boundary provides a means of estimating both the thickness and rheology of the crust at the time of formation. Such constraints are key to understanding the early thermal and chemical evolution of the planet.

[6] Despite the potential for gravitational relaxation, *Nimmo and Stevenson* [2001] find that lower crustal flow is not a significant factor in shaping the dichotomy boundary. They model a smoothed, averaged slope from 10 N-S profiles across the dichotomy using a depth-dependent, non-Newtonian model of crustal flow. Their results suggest that the crust must be between 30 and 100 km thick. One goal of this study is to examine a single area of the dichotomy in detail in order to constrain the effects of geologic history on the modification of the dichotomy. We will use these results to constrain future modeling of relaxation of the boundary, using the approach of matching the observed faulting types, locations, and strains, in addition to topography.

[7] We carry out a detailed examination of a section of the dichotomy from 50–90E. In this area, a series of boundary parallel fault scarps define the local edge of the dichotomy (Figure 1). We begin by examining the geologic history of the region, including the age of the major structural elements. Next we model the gravity field data to infer subsurface structure and estimate local crustal and elastic thickness at the time of loading.

[8] Additionally, there appears to be a correlation between the geology, gravity, and magnetic field data in this area. This correlation provides additional information about the subsurface structure along the dichotomy boundary as well as constraints on the thickness and modification of the magnetized layer that crosses the dichotomy. Discovery and mapping of the crustal remanent magnetic field on Mars [*Acuna et al.*, 1999, 2001; *Connerney et al.*, 1999, 2001] further illuminated differences between the lowlands and highlands. Although the dichotomy is not a sharp boundary in the observed remanent crustal magnetization anomaly field, the strongest magnetic anomalies are largely confined to the southern highlands, with a small number of localized, less intense magnetic anomalies found in the northern plains. Most of the lowland magnetic anomalies occur along the dichotomy boundary. Although a large portion of the southern highlands is magnetized, some regions apparently lack magnetization, notably the region south and west of the Hellas impact basin and south of the Argyre impact basin. The lack of correlation between magnetic anomalies, gravity anomalies, and surface geology in most areas of Mars has frustrated studies of the sources and origin of the magnetic field. Our study area may be unique in terms of the observed correlations. Thus an additional goal of the study is to use modeling of the gravity and magnetic field data to place constraints on the thickness and intensity of the magnetic sources in this area.

2. Background

2.1. Models for Origin

[9] A variety of endogenic processes have been proposed for the origin of the dichotomy. There are two models involving degree 1 mantle convection that have been offered as hypotheses for the origin of the dichotomy. In the spherically axisymmetric model of *Zhong and Zuber* [2001] and *Zhong et al.* [2000] applied to the Moon, an instability in the lowermost mantle causes heat to be lost preferentially in one hemisphere through an increased number of hot upwellings. The hottest lower layer migrates to this high heat flux hemisphere, leaving the other hemisphere relatively cold. Such an instability was reached after about 350 my in the example presented. Thus in this model for Mars, the northern plains represent a region of enhanced heat flow, consistent with both the younger age of the plains and the greater initial thickness of the southern highlands inferred from the large elastic thickness derived for the Hellas impact basin [*Zuber et al.*, 2000]. *Zuber et al.* [2000] have further suggested that high heat flow in a large

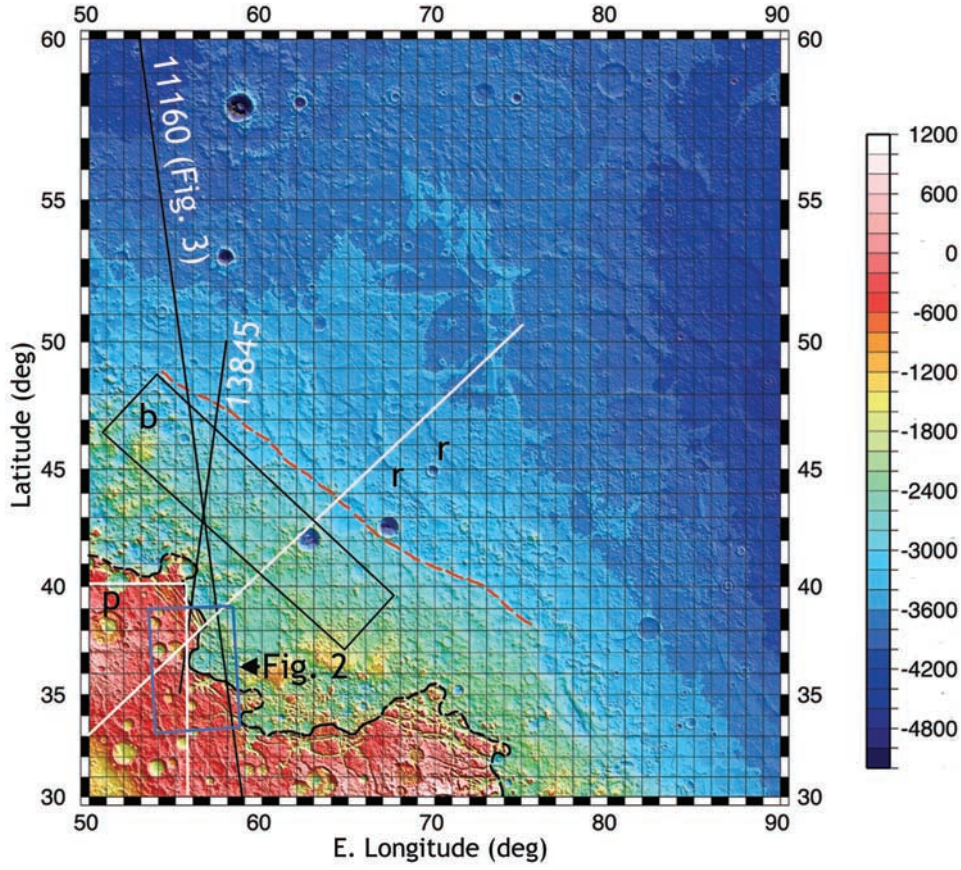

Figure 1. MOLA topographic image of study area in meters, gridded at 256 pxl/degree. Figure shows trace of MOLA track 11160 (Figure 3); MOLA track 13845, which is used to estimate extension across the grabens; the dichotomy boundary (irregular black line); trace of *Dimitriou*'s [1990] buried fault (dashed red line); and the location of Figure 2 (blue box). r, possible wrinkle ridges; box b (black box), area for lowland bench crater count (Figure 5); box p (white box), area for plateau crater counts (Figure 4). The plateau counting area extends westward to 45E, coinciding with the west limit of *Dimitriou*'s [1990] mapping. The white line shows the location of a profile though the magnetic field (Figures 8 and 10). Scale at right is elevation in meters.

region of Mars would have cooled the mantle sufficiently to reduce melt production later in Martian history.

[10] In the spherically axisymmetric model of *Breuer et al.* [1997], the two exothermic olivine-spinel phase transitions are included, introducing the competing effects of thermal buoyancy and latent heat release. The mass transport pattern oscillates as a result, yielding variable numbers of plumes. The overall slow cooling of the planet in this model will decrease the number of plumes. This model has been used to understand both the large Tharsis volcanic region and the periodicity of volcanism. Although not specifically proposed to explain the dichotomy, it could be applied in this way. A single plume or concentration of plumes in one hemisphere could have either produced very large volumes of crust, consistent with the formation of the southern highlands, or thinned the crust as suggested by *Zhong and Zuber* [2001] for their mantle instability model. A potential problem for this model is that hemispherical scale plumes do not develop until 1–2 b.y. into the evolution of the planet [*Breuer et al.*, 1998], although this delay is consistent with the timing of dichotomy formation proposed by *McGill and Dimitriou* [1990].

[11] Additionally, core formation may produce degree 1 mantle convection [e.g., *Schubert and Spohn*, 1990; *Stevenson*, 1980]. However, core formation is believed to occur very early in Martian history [*Chen and Wasserburg*, 1986], which appears inconsistent with the stratigraphic history of the boundary [*McGill and Squyres*, 1991]. Alternatively, early differentiation events may have led to asymmetries in the crust [*Breuer et al.*, 1993].

[12] A further endogenic hypothesis attributes the dichotomy to subduction of the northern plains under the southern highlands [*Sleep*, 1994]. Although *Zuber et al.* [2000] find that the region of the northern plains with a crustal thickness of 40 km coincides well with the region of crust occupied by spreading centers in Sleep's model, evidence for an Early Noachian age for most or all of the northern lowland basement [*McGill*, 1989; *Frey et al.*, 2002] effectively rules out the specific model proposed by *Sleep* [1994]. *Lenardic et al.* [2004] proposed an alternative role for plate tectonics. In their model, insulation caused by crustal thickening in the southern highlands leads to a decrease in mantle viscosity and thus a transition from active plate tectonics to a stagnant lid regime. Once a stagnant lid develops, little additional

crust forms, preserving the thickness differences between north and south.

[13] Most evidence to date does not favor an exogenic origin. One line of evidence is the lack of continuity in massif distribution, and irregularities in the boundary [*McGill and Dimitriou*, 1990; *McGill and Squyres*, 1991]. Although the edge of the dichotomy is clearly defined by impact basins in some regions (such as near Isidis and Utopia), the multiple impact hypotheses does not account for much of the low topography in the north [*McGill and Squyres*, 1991]. Further, there is no evidence from gravity data analysis that a single basin or a series of basins forms the dichotomy boundary [*Zuber et al.*, 2000].

2.2. Topography and Crustal Thickness

[14] The global MOLA data set has offered a variety of new insights into the nature of the dichotomy. *Smith et al.* [1999] demonstrate that the majority of the elevation difference between the southern and northern hemispheres, approximately 5 km, is due to the center-of-figure center-of-mass offset. They estimate that the average slope from the south pole to the north pole is 0.036°. *Smith et al.* [1999] thus conclude that most of the elevation change between hemispheres is a long-wavelength feature rather than a step function occurring at the boundary. However, a preliminary examination of the dichotomy by *Frey et al.* [1998] found that a steep, local change in slope provides a better fit to the topography than a long-wavelength slope. Clearly the dichotomy has both a long wavelength and a local scarp component. *Smith et al.* [1999] suggest that major contributions to the dichotomy come from the ejecta blanket surrounding Hellas, with possible contributions from Isidis and Utopia, and that the boundary may be highly modified by outflow channels flowing into Chryse Planitia. Although ejecta from Hellas certainly contributes to the local topography of the highlands, it does not explain the steep slopes along some sections of the dichotomy. Additionally, the analysis of *McGill* [2000] of the topography at Utopia suggests that the long-wavelength tilt of the dichotomy predates the youngest (Latest Hesperian and younger) materials in Utopia Plantia. The old limit on tilting is difficult to define, but the timing of the tilt with respect to the formation of the boundary plays a key role in determining the relationship, if any, between the two primary physiographic elements of the Martian surface.

[15] Analysis of gravity and topography data indicates that the mean thickness of the crust on Mars is on the order of 50 km and that the crust beneath the northern lowlands is typically 20–30 km less than beneath the highlands [*Zuber et al.*, 2000; *Zuber*, 2001]. An exception is the Arabia Terra section of the highlands in that its crustal thickness is more similar to that of the northern lowlands [*Zuber et al.*, 2000], despite its high crater density and intermediate elevation. Several studies have shown that areas along the dichotomy boundary are isostatically compensated [*Nimmo and Stevenson*, 2001; *McGovern et al.*, 2002; *McKenzie et al.*, 2002; *Nimmo*, 2002]. The dichotomy can be divided into three segments based on crustal thickness variations [*Zuber et al.*, 2000]: (1) the Arabia Terra region from 310–60E where the dichotomy boundary does not correspond to an increase in crustal thickness, (2) from 60–190E where the boundary coincides with the increase in crustal thickness from the lowlands to the highlands, except where interrupted by the Isidis basin, and (3) from 190–310E where the boundary is obscured in the Tharsis region. In this study we examine the dichotomy near the transition from section 1 to section 2.

2.3. Global Geologic Characteristics

[16] *Parker et al.* [1989, Figure 1] divided the Martian dichotomy boundary into segments that were identified as ''gradational'' or ''fretted''. This division remains generally valid, but not all of their fretted segments contain terrain fitting the definition of type fretted terrain [*Sharp*, 1973]. The boundaries in the segments labeled fretted are all defined by scarps, presumably caused by faulting, and thus ''scarped'' is preferred over ''fretted'' as a label. Of course, in some of these segments post-faulting erosion has created fretted terrain. A scarp defines most of the segment of dichotomy boundary in the Ismenius area, and thus comparisons with other scarped segments are of interest. Work in the Amenthes area [*Maxwell and McGill*, 1988], to the east of Isidis Planitia, indicated that the scarp defining the dichotomy boundary cut highland plateau materials after the plateau had been resurfaced in the Late Noachian. Furthermore, *McGill and Dimitriou* [1990] demonstrated that this scarp could not be due to extensive erosion at any time since the Early Noachian, using arguments similar to those used here for the Ismenius area. Specifically, the depth of erosion required would obliterate all old craters superposed on the lowland basement, yet craters are clearly still detectable. Thus the dichotomy boundary in the Amenthes area is a faulted boundary that has suffered only minor post-faulting erosion. *Frey et al.* [1988] studied a large segment of the dichotomy boundary from Amenthes westward to the type fretted terrain in north-central Arabia Terra. Their results consistently dated the highland plateau surfaces as Middle Noachian. They also derived crater ages of Middle Noachian to Early Hesperian for a transition zone on the lowland side of the boundary scarp. This transition zone includes a lowland bench found in our study area, as described below. Their result also requires that the current boundary scarp is not due to extensive erosion since the Early Noachian because, again, the craters used to derive the transition zone ages would have been completely obliterated by this erosion. Finally, *McGill* [2000, 2002] noted that the scarps bounding the plateaus and mesas of the type fretted terrain in north-central Arabia Terra are cutting a plateau surface that is Middle Noachian in age. The fretted terrain shows strong evidence for structural control of erosion [*Kochel and Peake*, 1984; *McGill*, 2000], requiring that the erosion forming the fretted terrain is Middle Noachian or younger. Thus in north-central Arabia Terra there apparently has been extensive erosion of the dichotomy boundary [*Phillips et al.*, 2001], unlike the situation eastward to Amenthes, a distance close to 180° of longitude [*Frey et al.*, 1988]. It is significant, however, that in the north-central Arabia Terra area the lowlands within the transition zone have not retained even a remnant of an old crater population superposed on the basement. Presumably, their absence is due to relatively young, extensive erosion of the boundary zone. Stratigraphic relationships in north-central Arabia Terra indicate that this extensive erosion most likely occurred in the Early Hesperian [*McGill*, 2000].

[17] Thus studies of a substantial fraction of the Martian dichotomy boundary indicate that scarps defining this boundary cut highland plateau materials of Middle to Late Noachian age. In most of the areas included in this substantial fraction of the boundary zone the boundary is defined by a fault, and the current scarp cannot have suffered extensive erosion since faulting. In north-central Arabia Terra the faulting was more pervasive, and the boundary zone has been extensively eroded there, perhaps because the complex of faults affecting the boundary zone enhanced erosional processes. What remains controversial is whether the dichotomy already existed when these boundary faults formed, as would be the case if the dichotomy were due to primordial differences in crustal thickness or due to giant impact, or if the Middle to Late Noachian boundary faults developed as part of the process that created or modified the dichotomy boundary [*Watters*, 2003a, 2003b].

2.4. Local Geology

[18] Between Isidis and Acidalia Planitiae the boundary between the southern highlands and the northern lowlands of Mars (the dichotomy boundary) follows a broad, north-convex arc. This arc approximately coincides with the northern limit of the large highland region Arabia Terra, and it includes the most northerly portion of the dichotomy near the crater Lyot where the boundary extends as far north as about 45N (depending on exactly where one places it). Arabia Terra is somewhat anomalous in that it consists of typical highland terrain yet its elevation is lower than most highlands. However, we will refer to Arabia Terra as highlands because it is significantly higher than adjacent typical lowlands terrain, and because it consists of highland-type terrain. The boundary and the adjacent Arabia Terra terrain in this region have received extensive study by many persons. Most of these studies address issues not directly related to the topic of this paper because the materials and processes considered clearly are younger than the dichotomy boundary. Nevertheless, they are relevant to the extent that they help us understand the modifications that have affected the boundary zone since formation of the dichotomy.

[19] Relevant prior work includes both global and quadrangle-scale geological mapping [*Scott and Tanaka*, 1986; *Greeley and Guest*, 1987; *Lucchitta*, 1978; *Dimitriou*, 1990], local to regional studies of fluvial and possibly lacustrine or marine erosion and deposition [*Lucchitta*, 1978; *Craddock and Maxwell*, 1993; *Hynek and Phillips*, 2001; *Parker et al.*, 1989; *Edgett and Parker*, 1997], local to regional studies of aeolian erosion and deposition [*Grant and Schultz*, 1990; *Moore*, 1990; *Tanaka*, 2000], deposition and stripping of mantling deposits [*Maxwell and McGill*, 1988; *Grant and Schultz*, 1990], mass wasting [*Sharp*, 1973; *Squyres*, 1979], volcanism [*Carruthers and McGill*, 1998], impact-crater modification [*Grant and Schultz*, 1990; *Craddock and Maxwell*, 1993], and overall crustal evolution [*McGill*, 2000].

3. Analysis

3.1. Geologic History

[20] The segment of dichotomy boundary selected for this study lies mostly within the 1:2,000,000 Ismenius Lacus SE and Cassius SW subquadrangles, where the dichotomy is generally well defined and locally characterized by a distinct scarp. This segment of the dichotomy boundary roughly coincides with the region referred to as "Protonilus Mensae". An important objective is to constrain the interval of relative time during which the dichotomy formed in this area, as opposed to when it was modified by deformation, volcanism, deposition of sediments, and erosion.

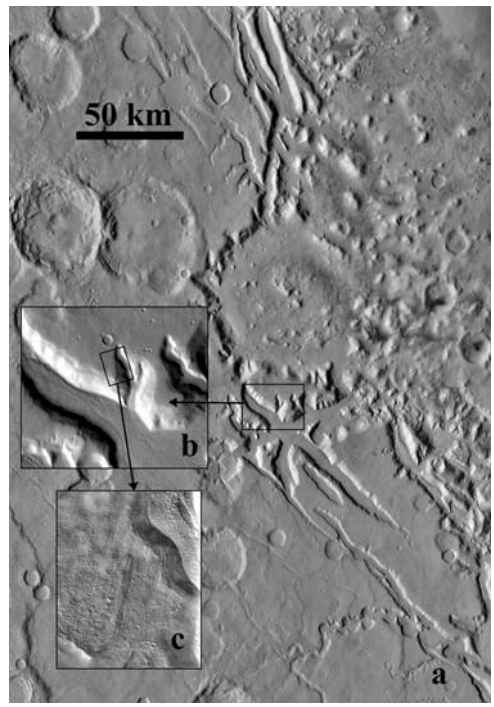

Figure 2. Structure of the dichotomy boundary between 56 and 59E. (a) Mosaic of Viking images 569a17-20 showing a complex of grabens cutting the highland plateau west and southwest of the boundary scarp. Box outlines area of Figure 2b. (b) Portion of Themis daytime infrared image I02220009 showing coarse layering in graben walls. Box outlines area of Figure 2c. (c) Portion of MOC image M0805662 showing multiple, fine-scale layers in valley wall. These images indicate that the graben faulting and subsequent valley formation are younger than the Middle Noachian layered materials capping the highland plateau.

[21] Specifically the area included in this study lies between 30 and 60N and between 50 and 90E. Within this area, the terrains along the dichotomy boundary can be separated into 3 structural blocks on the basis of surface morphology and elevation. The three blocks are, from southwest to northeast: highland plateau, lowland bench, and lowland plains (Figure 1). Between 50 and 60E the highland plateau and lowland bench are separated by a northwest-trending scarp that averages ~2.5 km in height and that is parallel to a set of large, deep grabens that cut the plateau material immediately southwest of the scarp (Figure 2). A similar boundary scarp in Amenthes has been interpreted as due solely to erosion [*Hiller*, 1979]. Although the 20° scarp slope indicates erosional modification of the probable primary slope of ~60°, we interpret the scarp to result from a major fault, down on the northeast, for reasons that will be discussed below. The present slope of this scarp ranges

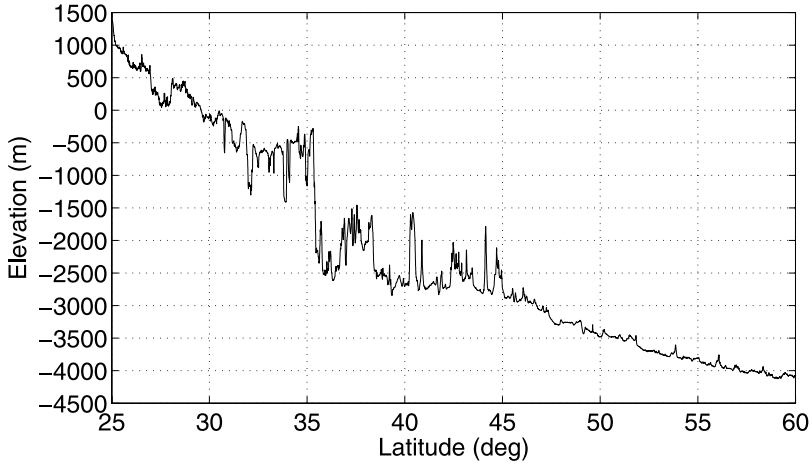

Figure 3. Topographic profile from MOLA orbit 11160 showing highland plateau, lowland bench, and lowland plains blocks. Although the lowland bench is horizontal overall, it is characterized by abundant high-frequency topography. At least 1 km of additional plains cover is required to account for the abrupt loss of this high-frequency topography north of 45N, which implies at least 1 km vertical displacement on the buried fault at the lowland bench/lowland plains boundary.

between 20° and 23°. West of 50E the dichotomy boundary lies within or adjacent to the type fretted terrain [*Sharp*, 1973], and its original position most likely lies near the northwest and north limits of fretted terrain [*McGill*, 2000, 2002]. Eastward from 60E the dichotomy boundary curves into a more east-west orientation and is characterized by significant disruption of the highland plateau adjacent to the boundary and by a complex zone, several hundred kilometers wide, of smaller elevation drops separated by a general northerly slope that, although gentle, is steeper than the ~0.036° northerly slopes that characterize much of Mars [*Smith et al.*, 1999]. The total relief across this complex east-west segment of the boundary zone is generally more than the ~2.5 km of relief across the well-defined boundary scarp between 50 and 60E.

[22] The boundary between the lowland bench and the lowland plains is defined by a contrast in topographic detail; abundant knobs separated by smooth plains material characterize the lowland bench, whereas knobs are rare to absent in the lowland plains block. The change from abundant knobs to rare knobs is abrupt. This boundary is approximately parallel to the scarp separating highland plateau from lowland bench, and thus is interpreted to represent the trace of a buried fault that also is down on the northeast [*Dimitriou*, 1990]. The inference is that the knobby surface of the lowland bench has been dropped to a lower elevation to the northeast and covered by a thicker layer of plains materials, thus masking the knobs. As is the case for much of Mars, the surfaces of the highland plateau and lowland plains blocks slope very gently toward the northern lowland (angle is much less than 1°); but for most of its width the lowland bench is essentially horizontal (Figure 3).

[23] MOLA topography further reveals the presence of ridges partially buried under plains material. Two of these ridges are parallel to the original fault from 80E to about 66E; westward from there they curve to a more N-S orientation, oblique to the fault and to the dichotomy boundary (Figure 1). These ridges have the sinuous character of wrinkle ridges, but are not expressed well enough to be clearly identified. Wrinkle ridges are widely distributed on Mars and commonly reflect local to regional stress systems. Below we suggest that the ridges northeast of the fault may be part of the dichotomy modification process.

[24] *Watters* [2003a, 2003b] has mapped and analyzed lobate scarps in highland terrain 200–300 km south of the dichotomy boundary in the Ismenius region. These scarps are interpreted to be formed by compressive stresses. The lobate scarps are parallel to the dichotomy boundary in the Ismenius area, and thus may be related to the processes responsible for the boundary. However, west of the Ismenius area the dichotomy boundary changes trend from NW to NE, whereas the lobate scarps do not [*Watters*, 2003a, Figure 1; *McGill*, 2002], suggesting that the common trend of lobate scarps and the dichotomy boundary in the Ismenius area could be coincidental. The age of the lobate scarps relative to the dichotomy boundary faults also is not well constrained; both types of structures apparently deform the same highland plateau material and thus have similar old age limits, but, unlike for the boundary faults, there is no way to constrain the young age limit for the formation of the lobate scarps. The lobate scarps indicate that NE directed compressive stresses existed at some time in the history of the Ismenius area, but the relationship of these stresses to the formation of the dichotomy boundary is problematical.

3.1.1. Strain Estimates Across the Dichotomy Boundary

[25] We use the set of grabens just SW of the dichotomy boundary near 39N, 54E to estimate the strain across the dichotomy boundary in this area. The slope on each graben wall is measured using MOLA topography from orbit 13845 (see Figure 1 for location) and corrected for the oblique intersection. The measured range of slopes is 13° to 21°, indicating that the graben scarps are very degraded as compared to the ~60° slope expected for pristine normal faults. We estimate the horizontal extension across each of 10 graben-bounding faults using the measured apparent vertical offset (scarp height) and assuming an original fault dip of 60°. Correcting both the total extension and the width

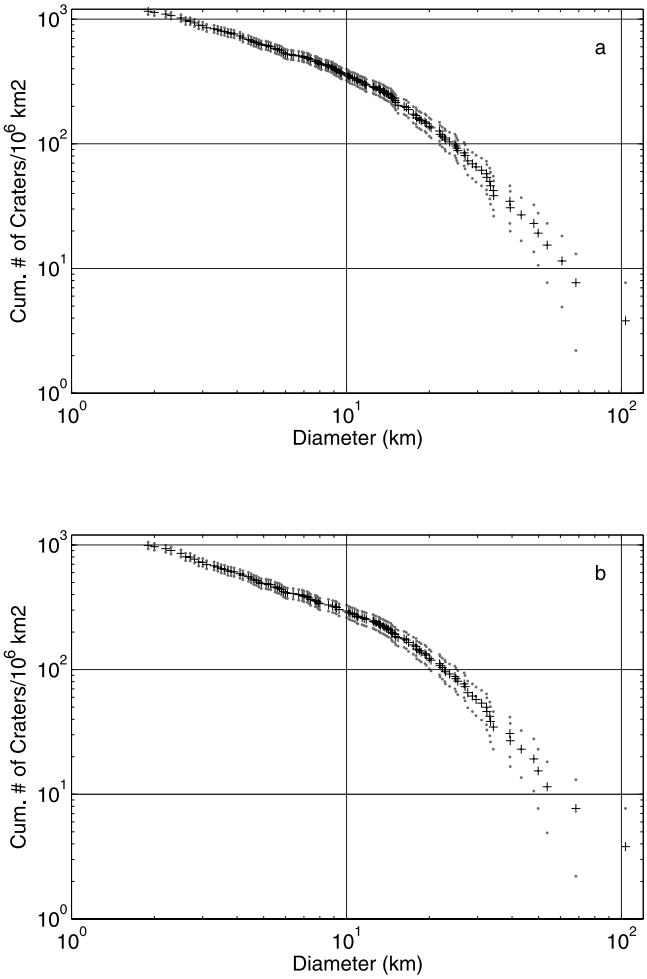

Figure 4. (a) Log diameter versus log cumulative number of all craters ≥2 km in diameter within a large area of plateau (Figure 1). Both the n (16) and n (5) numbers [*Tanaka*, 1986] indicate a late Early Noachian age for the basement beneath the plateau surface. Crosses are cumulative numbers, dots 1-σ error limits; n = 293. (b) Count within same area as Figure 4a, but limited to craters ≥2 km in diameter superposed on plateau surface materials. The n (16) and n (5) numbers imply a Middle Noachian age; n = 258.

of the graben bundle along the MOLA orbit for the 50° intersection angle between the profile and graben trends yields a current width of the graben bundle of 50.5 km, and an apparent extension of 1.73 km. For just the area of the grabens this is a 3% strain. The current graben depths are likely shallower than the original depths since the material eroded from the walls to yield the low current slopes was probably deposited on the graben floors. If so, these numbers are likely a lower bound. If we include the boundary scarp itself, the total estimated strain is 3.5%. Although this scarp is ∼2.5 km high (as measured on MOLA profiles 11160 and 13845), several times higher that the graben walls, the baseline over which to calculate the strain is much larger (∼100 km rather than ∼50 km). The 3.5% strain is just for the width of the faulted area, and thus the total extension across the entire ∼450 km wide zone between the boundary scarp and the buried fault would be much less, unless there is very significant extension across buried faults on the lowland side of the boundary. Even if we assume a comparable vertical offset between the ∼2.5 km high scarp and the buried fault and perhaps even across one or two others like it within the bench area, the overall extension is likely much less than 3.5%.

3.2. Age of Units

[26] *Dimitriou* [1990] subdivided the highland plateau into several units based on surface characteristics resulting from later erosional or deformational processes. The basement materials underlying the surfaces of these plateau units are of similar age [*Dimitriou*, 1990], and thus for this study crater ages are determined for a single large area (265,000 km^2) of highland plateau. Highland craters of all degradation states have been counted within this area. This count yields a late Early Noachian age (Figure 4a). If only craters superposed on the plateau surface material are included, the age is Middle Noachian (Figure 4b), which is thus the age of the material capping the plateau. As pointed out by *Dimitriou* [1990], the crater plots are complex, suggesting modification of the plateau surface material since its emplacement in the Middle Noachian, but this does not invalidate the Early and Middle Noachian ages, which are based on large (diameter ≥16 km) craters.

[27] The lowland bench is noteworthy for its abundant knobs, some of which define circles or parts of circles and thus are likely to be remnants of fractured and eroded crater rims. The knobs are inliers showing through a much younger smooth plains material. A count for a large area (170,000 km^2) of lowland bench yields a crater age of Late Noachian (Figure 5). It is apparent that old craters on the bench have been subject to greater tectonic disruption than craters on the adjacent highlands, as indicated by the disruption of the rims of old craters into knob rings on the bench in contrast to the subdued but generally unbroken rims of old craters on the plateau. Both basement surfaces have undergone younger modification by erosion, but the

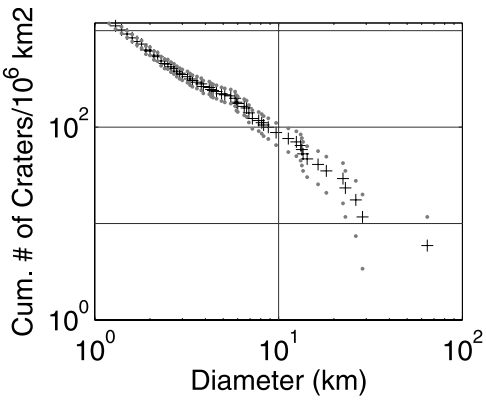

Figure 5. Log diameter versus log cumulative number of craters ≥0.7 km in diameter within a large area on the lowland bench (Figure 1). Both the n (16) and n (5) numbers [*Tanaka*, 1986] indicate a Late Noachian age, which is inferred to represent a minimum age because of loss of craters due to tectonic disruption and burial by plains materials; n = 274.

lowland bench has also been covered with a veneer of young plains materials; comparably young materials on the highland plateau are very local in occurrence. The greater tectonic disruption and thicker plains cover result in loss of many of the oldest and most degraded craters on the basement surface beneath the bench. We thus infer that the basement beneath the lowland bench is most likely Early Noachian in age, similar to the basement beneath the highland plateau. The probable presence of buried craters and small basins beneath the lowland bench and plains surface material [*Frey et al.*, 2002] also supports an Early Noachian basement beneath both the lowland bench and lowland plains, similar to the basement beneath the highland plateau.

[28] The smooth plains material between the lowland bench knobs extends into valleys and graben incised into the adjacent highlands, and thus these structures must be older than smooth plains. It is not possible to obtain a robust crater age for the smooth plains material close to the highlands, but a crater count of the entire area of smooth plains mapped by *Dimitriou* [1990] yields ages between Late Noachian and Late Hesperian. The younger age is preferred because at least some of the larger craters included in the count are probably beneath the smooth plains rather than superposed on them. *Frey et al.* [1988] defined and described a transition zone between highlands and lowlands that includes our lowland bench block. Using a curve-splitting technique proposed by *Neukum and Hiller* [1981], crater counts for the transition zone west of Isidis basin yielded Late Noachian and Late Hesperian ages, in agreement with the results of *Dimitriou* [1990]. Curve splitting explicitly implies the presence of older and younger crater populations, and thus the results of *Frey et al.* [1988] support the presence on the lowland bench of Late Hesperian cover material on a Noachian basement. Plots for smooth plains from *Frey et al.* [1988] indicate a Late Hesperian age as well, and curve-splitting has little effect on the derived age for smooth plains. These data suggest that the smooth plains between the knobs on the lowland bench are similar in age to smooth plains on the lowland plains block; the primary difference is that the smooth plains on the lowland bench block are thinner than the smooth plains on the lowland plains block and thus expose a larger population of partially buried craters on the underlying basement surface.

3.3. Origin of the Boundary Scarp

[29] Is it possible that the 2.5 km of relief between the highland plateau and the lowland bench is entirely due to erosion? One possible interpretation would have this erosion occur in the Early Noachian so that the apparent similarity in basement ages between the plateau and bench would be due to the post-erosion impact history. There are two problems with this model: (1) the scarp separating highland plateau and lowland bench cuts Middle Noachian plateau surface material (Figure 2), and (2) the well-defined scarp could not possibly have survived major bombardment in the Early Noachian. A second model would have the erosion occur after emplacement of the Middle Noachian plateau material, and thus after the emplacement of most of the craters defining the ages of the basement and plateau cover material. But, based on the crater morphometric models of *Pike and Davis* [1984], 2.5 km of erosion would obliterate the rims of all craters and basins with diameters less than ~1,500 km, and would erode the basement surface deeply enough that not even crater depressions would remain for craters smaller than ~90 km in diameter. The equations of *Garvin et al.* [2003] yield comparable results. This erosion would have destroyed all of the craters defining the Noachian basement age for the lowland bench. These considerations rule out erosion as the primary cause of the boundary scarp in the Ismenius area.

[30] We thus believe that explaining the boundary scarp as due to faulting is a robust interpretation, not only because a strictly erosional model is so improbable, but also because of support provided by the large grabens that are adjacent and parallel to the boundary scarp. The 2.5 km of relief across the boundary scarp provides a minimum estimate of vertical displacement on the fault responsible for the scarp. Erosion of the plateau surface on the footwall of this fault and deposition on its hanging wall would lead to an underestimate of the original relief across the fault. No evidence is apparent in the images for significant lowering of the plateau surface since faulting, and post-fault deposits on the bench appear to be thin (40–50 m), based on surviving relief of craters superposed on the underlying basement. Thus we will assume that 2.5 km is a good estimate of fault displacement. Estimating the displacement across the buried fault between the lowland bench and lowland plains is more difficult. However, the abrupt loss of high-frequency relief across the bench-plains boundary provides a means to determine a minimum vertical displacement. Because the present lowland surface changes from horizontal to gently sloping in a zone that includes this boundary with no abrupt elevation change, the abrupt loss of high-frequency topography is most likely due to a greater thickness of young deposits on the lowland plains side of the boundary. Thus the displacement across the buried fault must be at least sufficient to account for the abrupt loss of high-frequency topography. At least 1 km of vertical displacement is needed to bury this high-frequency topography (Figure 3), and we thus accept this as the minimum displacement on the buried fault.

[31] A key question is when the faulting responsible for the scarp and lowland bench/lowland plains boundary occurred. The scarp and the grabens cut the plateau surface material, and thus must be Middle Noachian or younger. The young limit is provided by smooth plains material that embays and thus is younger than the fault scarp, and that buries the buried fault. The age of this smooth plains material is difficult to pin down exactly, but is most likely Late Hesperian. Using the chronology model by *Hartmann and Neukum* [2001], these limits would place the faulting between about 3.9 and 3.1 Ga. *Frey* [2004] estimates that the dichotomy had formed by 4.04 to 4.20 Ga, also using the *Hartmann and Neukum* [2001] chronology. These age estimates imply that scarps along the dichotomy boundary formed within 0.14–1.1 Gyr after the dichotomy boundary.

4. Gravity and Magnetic Field Data Analysis

[32] In this section we use the gravity and magnetic field data as further constraints on the subsurface structure and on the compensation mechanism in this region. Our analysis is

carried out using 85 degree and order topography and gravity fields, computed out to degree and order 50 to prevent the aliasing of high-degree noise into the gravity field. The specific gravity field we use is MGS85H, which is an update from the published field [*Yuan et al.*, 2001], computed relative to the center of mass with a mean planetary radius of 3389.5 km [*Smith et al.*, 1999]. The topography is computed using the same reference frame and to the same degree and order. For the magnetic field analysis, we use a data set constructed as an average of three independent representations of the magnetic field data (M. Purucker, personal communication, 2003): two spherical harmonic models of the vector field (one to degree and order 90 [*Cain et al.*, 2003] and one to degree and order 65 [*Arkani-Hamed*, 2002a]), and the equivalent point source model of the low-altitude radial field calculated at 200 km [*Purucker et al.*, 2000]. The averaged map is calculated at 120 km altitude to resolve features detected by the low-altitude aerobraking and science phasing orbit data, much of which was collected below 120 km. *Cain et al.* [2003] have compared the three models and found good agreement, except amplitudes in their models are generally larger at the shortest wavelengths; thus the spatial averaging may have reduced the amplitudes at the shortest wavelengths. The main features interpreted here are common to all the field representations. The radial and theta components of the anomaly map from the averaged 120 km model are shown in Figures 6a and 6b, respectively, along with the total anomaly in Figures 6c and 6d. The magnetic anomaly components are presented as color contour maps, with contoured long-wavelength topography (Figures 6a and 6b) and the contoured Bouguer gravity (Figure 6c) and free-air gravity (Figure 6d) fields superimposed. A profile was extracted from the 120-km average field that crosses the dichotomy boundary, the lowland bench, and the buried fault to the north, indicated by the magenta line. The buried fault is shown as a black line.

4.1. Gravity, Topography, and Magnetic Field Description

[33] There is not an exact correspondence between the gravity anomalies and the total field magnetic anomalies, but south of ~50N many of the peaks in the magnetic anomaly field occur within several degrees of peaks in the free-air gravity field (Figure 6c), suggesting the possibility of common sources of density and magnetic anomaly variations in this region. Sharp gradients in the gravity field occur across the buried fault (white line in Figure 6), indicating a change in density across the fault. A large positive gravity anomaly occurs in the upper left of this region (Figures 6c and 6d). This anomaly extends further to the north, where there is no evidence of magnetized crust. In the northeast corner of this region, there is a strong positive anomaly that is contiguous with the gravity low over Utopia Planitia. These two regions are among the largest positive gravity anomalies in the northern plains [*Zuber et al.*, 2000]. These anomalies appear to be related to processes that are centered outside of the study area and are not discussed further.

[34] The dominant feature of the long-wavelength topography (expanded to degree and order 50) is clearly the dichotomy boundary (Figures 6a and 6b). Several other features are worth noting in addition. The lowland bench defined in Figure 1 contains a low that extends out to and wraps around the magnetic anomaly just to the northeast of the buried fault, near 43N, 61 E (Figures 6a and 6b). To the northeast of the buried fault, the plains are slightly elevated in the center of the area where magnetic anomalies in the plains have highest amplitude. The western edge of Utopia Planitia corresponds to the eastern section of this area. The elevations in this area slope eastward into the Utopia basin.

[35] The location of subsurface density anomalies can be seen in the Bouguer gravity anomaly (Figure 6d). The Bouguer gravity is the gravity signature predicted by the topography, using the relationship $2\pi G\rho$, where G is the gravitational constant and ρ is the density of the crust near the surface. Using the long-wavelength topography (Figure 6b), the Bouguer anomaly (Figure 6d) is computed by removing the Bouguer gravity from the observed gravity. We use a density of 2900 kg/km^3 for the crust, consistent with a basaltic composition. The largest peaks in the Bouguer anomaly are located over the highlands. These large negative anomalies reflect the increase in crustal thickness compensating the highlands topography. The Bouguer anomalies in the plains (Figure 6d) are reduced in magnitude from the free-air gravity (Figure 6c), but have a similar pattern. Since there is little topography in the plains relative to the highlands, there is not as large a difference between the Bouguer gravity and the free-air gravity in the plains as there is in the highlands.

[36] The magnetic and Bouguer gravity anomalies are reasonably well correlated over the lowland bench (Figure 6d). The Bouguer gravity anomaly over the lowland bench is clearly more positive southwest of the region bounded by the buried fault, relative to the adjacent lowland areas to the northwest and southeast. The large gravity and magnetic anomalies to the northeast of the buried fault are also reasonably well correlated, although there is an offset in the peak values that could be explained by a non-vertical magnetization vector. Over the center of the lowland bench and northeast of the buried fault, the magnetic anomalies are correlated with positive Bouguer anomalies, indicating positive density anomalies at depth. In the highlands region south of the dichotomy, and in the plains in the southeast corner, there is some correspondence between the gravity and magnetic anomaly peaks, such as near 37N, 83E and 39N, 75E. However, the relationships in these areas appear more complex than in the vicinity of the buried fault. The crustal compensation of the highland plateau may obscure other density variations. In subsequent analysis, we focus on the areas in the vicinity of the buried fault, where we have the most information on subsurface structure and geologic history.

4.2. Gravity Analysis

[37] We can investigate the gravity signature of an anomalous crustal layer by calculating the isostatic anomaly. The isostatic anomaly calculation removes the gravity signature of a subsurface crustal layer from the Bouguer gravity, assuming that the layer provides isostatic compensation of the topography. Admittance analysis of this region, discussed below, supports the validity of the isostatic assumption. The isostatic anomaly for a layer with a thickness of 50 km is shown in Figure 7a. Under the highlands area the

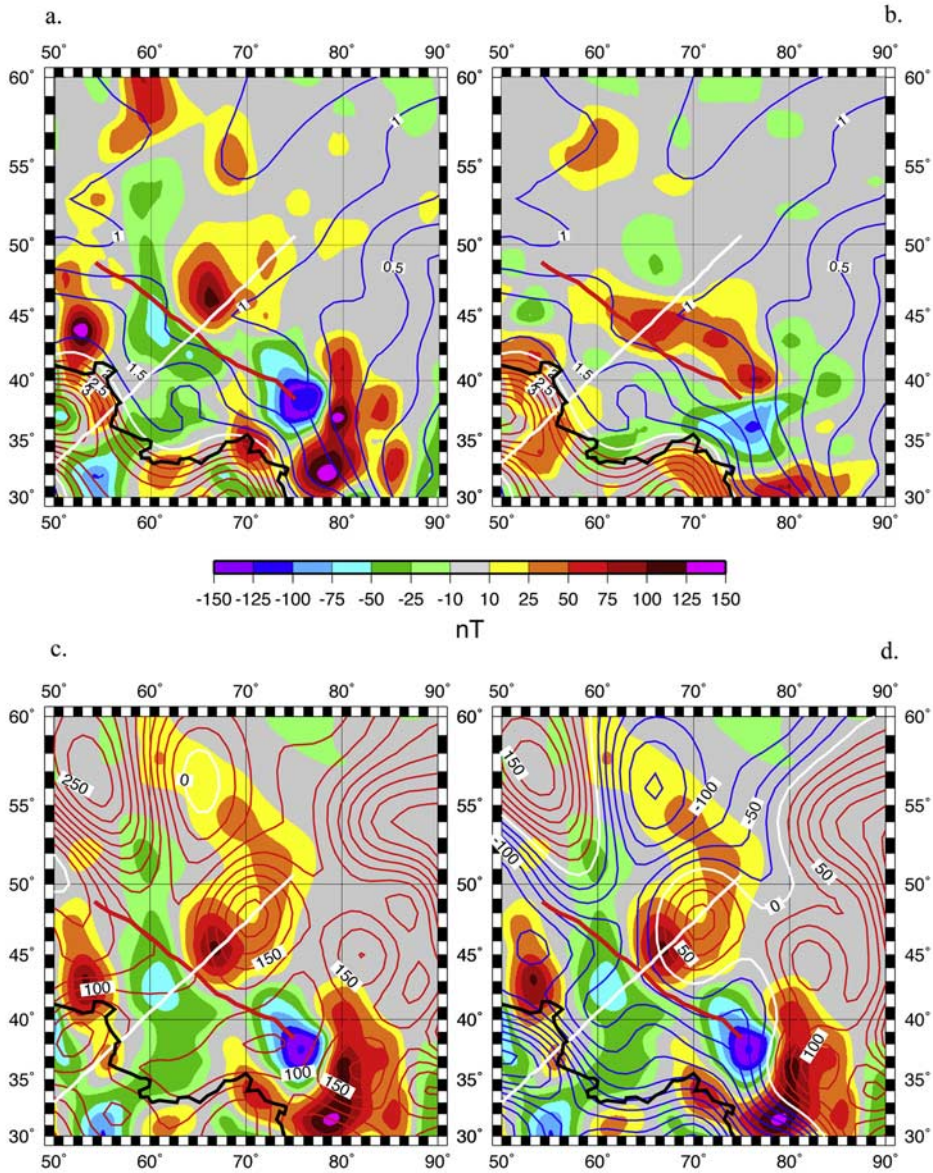

Figure 6. The magnetic field in the study area is shown as a color map background image along with superimposed contoured gravity and topography. The magnetic contour scale is shown in the center. The long-wavelength MOLA topography (degree and order 50), contoured at 0.2 km, is shown along with the radial and theta magnetic field components in Figures 6a and 6b, respectively. Elevations higher than 2.0 km contour (white contour) are shown in red, while those lower are shown in blue. The total magnetic field is shown in Figures 6c and 6d, along with contours of the free-air and Bouguer gravity in milligals in Figures 6c and 6d, respectively. Red contours are positive, zero is white, and negative is blue. In each panel the buried fault is shown as a red line, the white line indicates the position of a magnetic profile obtained by sampling the gridded data, and the dichotomy boundary is the black line.

isostatic anomaly is small. This is consistent with past work, suggesting a planetary average crustal thickness of ~50 km [*Zuber et al.*, 2000] and thickness in the range of 30–100 km in the southern highlands [*Nimmo and Stevenson*, 2001; *Nimmo*, 2002; *McGovern et al.*, 2002]. In the lowlands, the choice of crustal thickness does not significantly affect the isostatic anomaly, as there is little topography to be compensated. Given the large gravity anomalies in the plains, it is not possible to strongly constrain the local crustal thickness in this area, since the large positive values tend to drive estimates toward unreasonably large values. The presence of a crustal layer (however thick) does result in larger positive density anomalies in the isostatic anomaly relative to the Bouguer anomaly, since even more dense material is needed to balance the negative contribution to the gravity from the low-density crustal layer. For example, the positive anomaly northeast of the buried fault goes from approximately 50 mgals in the Bouguer anomaly

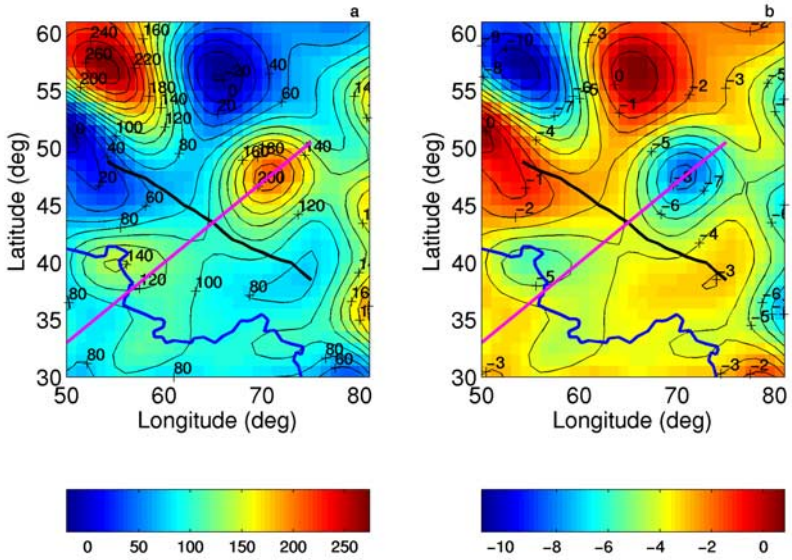

Figure 7. The isostatic anomaly (in milligals) resulting from removing the gravitational contribution of the topography and a 50 km thick crust (Figure 7a). Remaining variations in the gravity field are represented as variations in the thickness of the crust in kilometers in Figure 7b. Light blue regions indicate 2–4 km of crustal thinning, red areas are 2–4 km of crustal thickening, and dark red areas have 6–8 km of crustal thickening. The magenta line indicates the location of the modeled magnetic field profile. The black line shows the position of the buried fault. The blue line indicates the location of the dichotomy boundary.

(Figure 6d) to 200 mgals in the isostatic anomaly (Figure 7a). Similarly, negative density anomalies are smaller in the isostatic anomaly relative to the Bouguer anomaly.

[38] One approach to interpreting the isostatic anomalies is to assume that they represent variations in the thickness of the crustal layer. Assuming a 50 km thick crustal layer overlying a mantle layer that is 600 kg/km^3 denser, we calculate the variations in the thickness of the crust that would be required to produce the observed isostatic anomalies (Figure 7b). The average variations in thickness are small under the highlands since a 50 km thick crust provides essentially complete compensation. Under the lowland bench (see Figure 1 for location) the equivalent layer thickness is approximately 4–5 km thinner. To the northeast of the buried fault, where the magnetic anomaly generally correlates with the positive density anomaly, the layer is up to 8 km thinner. Directly under the buried fault the thinning is reduced to about 3 km. Smaller (larger) density contrasts between the crust and mantle produce larger (smaller) variations in the thickness of the layer. The relationship between density and the equivalent layer thickness variation is linear, so a density contrast of 300 kg/m^3 requires twice as thick a layer to produce the same gravity anomaly. If we vary the thickness of the assumed crustal layer, the amount of thinning or thickening required to produce a given isostatic anomaly will vary due to the R^2 dependence of the gravity field, where R is the distance between the mass and the point at which the gravity field is measured.

[39] Given the possible association between the gravity and magnetic field anomalies across the buried fault, we investigate the hypothesis that within the crust there is an additional, magnetized layer with a higher density than the nominal crust. To illustrate this, we take a profile through the isostatic anomaly field parallel to the magnetic profile shown in Figure 1. The isostatic anomaly has a peak just north of the dichotomy and north of the buried fault near 47N, 69E (Figure 8a). The isostatic anomaly peaks are approximately 200 km north of the peaks in the magnetic field data (Figures 8a and 8b). In Figure 8c we show the thickness of a layer that produces the observed isostatic anomalies for a range of density contrasts. These thicknesses are somewhat underestimated, especially for larger layer thicknesses, as they do not take into account the R^2 dependence of the gravity field, but are intended to illustrate the trade offs. For a layer approximately 10 km thick, a density contrast of 300 kg/m^3 is needed. For a layer with an average thickness of roughly 30 km, a density contrast of 100 kg/m^3 reproduces the observations.

[40] Modeling of the admittance signature of this region indicates that this region is likely isostatically compensated. The admittance is the transfer function between the gravity and the topography as a function of wavelength. It is used to estimate the crustal and elastic thickness of specific regions. The general theory of admittance modeling is described in numerous papers [e.g., *McGovern et al.*, 2002; *McKenzie et al.*, 2002; and references therein]. Here we use a section of the gravity and topography fields (50–81E, 30–61N) derived from the spherical harmonic coefficients to calculate the admittance for this region. The admittance curve is modeled as a top-loaded lithosphere, based on the positive slope of the admittance at short wavelengths (see Figure 9a). The RMS error in the observed admittance spectra is 7.2 mgals/km. The error analysis, which shows the trade off in the fit for various values of crustal and elastic thickness, is shown in Figure 9b. The specifics of this approach to calculating the admittance, estimating the

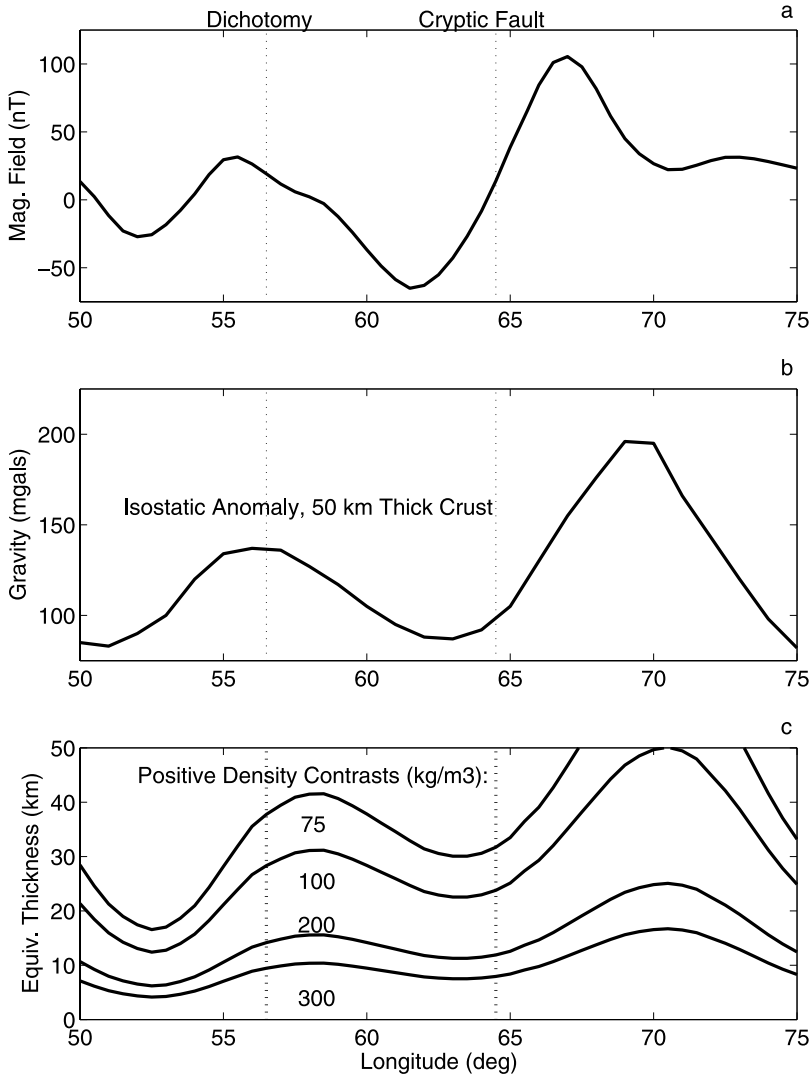

Figure 8. Figure 8a shows the magnetic profile from the location indicated in Figure 1. A profiles through the isostatic gravity anomaly parallel to the magnetic field profile is shown in Figure 8b. The thicknesses of layers with varying density contrasts that would produce an equivalent gravity anomaly are shown in Figure 8c.

model parameters, and the error analysis are described by *Smrekar et al.* [2003]. As seen in the error analysis, the best fit values of crustal thickness and elastic thickness are 25 km and 10 km, respectively. For a ratio of the RMS observed to the RMS of the model fit of 1.5, crustal thicknesses of 10–30 km and elastic thicknesses of 0–15 km also provide an acceptable fit to the data. This method of accounting for errors in the calculated admittance spectra and the fit in the data also includes an allowance for errors in the gravity and specific crustal densities. Assuming an RMS fit to RMS observed ratio of 2, the crustal thickness estimate changes to 5–35 km. The estimate of elastic thickness is essentially unchanged. The value of elastic thickness, which includes the 0 km value, is consistent with other estimates of the elastic thickness in highland areas [*Nimmo*, 2002; *McGovern et al.*, 2002]. As in other studies, we interpret this low value to indicate that this region is largely isostatically compensated. The value of crustal thickness we find falls within the range found by *Nimmo* [2002] for the highlands, and is somewhat lower than that found for some highland areas by *McGovern et al.* [2002]. This may be due to the fact that the area modeled includes a large section of plains. As noted above, the exact thickness of the crust in this region can not be well constrained due to significant anomalies that do not appear to be a result of crustal thickness variations alone.

4.3. Magnetic Field Modeling

[41] Modeling of the magnetic anomaly field offers additional insight into the subsurface structure. Simple 2-D forward models of crustal zones or blocks with coherent magnetization are used to investigate possible sources of the observed magnetic field, sampled along the profile indicated in Figure 6. Our approach is to assume a single intensity and inclination of magnetization for all of the sources in each individual model, and vary the source

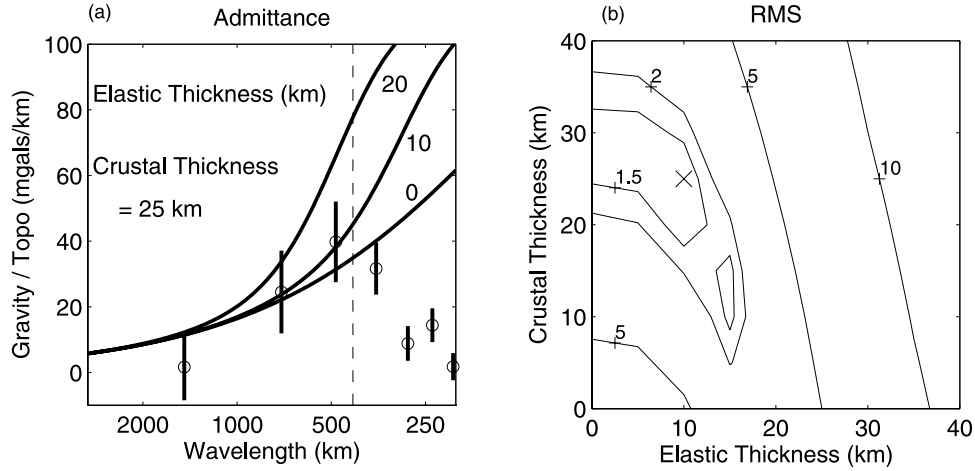

Figure 9. The admittance data with error bars are shown in Figure 9a, along with three models of compensation assuming a crustal thickness of 25 km and elastic thicknesses of 0, 10, or 20 km (solid lines). The vertical dashed line indicates the local resolution limit in the gravity data. The error analyses for models with elastic and crustal thicknesses in the range of 0–40 km are shown in Figure 9b. Each contour is the ratio of the observed RMS error in the admittance data over the RMS model fit. Models are run at 5 km intervals in elastic and crustal thickness.

dimensions and positions to achieve a good fit to the observed profile. Under the assumption of a constant direction of magnetization, the lateral placement of the source bodies depends on the assumed paleofield inclination. The thickness of the sources varies nearly inversely with the assumed intensity of magnetization. The r^3 dependence of the magnetic field on the distance to the source, r, means that the predicted model amplitude is very sensitive to the depth of the anomaly. However, thickness and intensity trade off such that their effects cannot be determined independently with the available data.

[42] Paleopole estimates for Mars derived from the anomaly field place both normal and reversed polarity poles in a region centered at 230E, 25N [*Arkani-Hamed*, 2001], or in a region centered at 225W, 50N [*Hood and Zakharian*, 2001]. The uncertainties on the paleopole estimates allow a wide range of possible inclinations for the study area, but exclude steep paleofield inclinations (>±60°) in our study area. The range of paleolatitudes expected across the sampled profile for the Arkani-Hamed poles is 10–30° ± 30° and 25° to 40° for *Hood and Zakharian* [2001]. The paleofield inclination variation (upper bound of 20°) across our study region is not taken into account, but this should not significantly affect the conclusions.

[43] Figure 10 shows four 2-D models with different source layer distributions and inclinations. Each panel shows the source bodies at the bottom, referenced to the location of the buried fault at 0 km, and the location of the dichotomy boundary (vertical dotted line). The predicted anomaly in nanoteslas (nT) is shown as a dotted line, and compared to the observed profile (solid black line). At the top of each panel, the isostatic gravity anomaly is shown by the dashed line. In this region of the dichotomy boundary, the parallel nature of the major structural elements, including the dichotomy itself, the lowland bench, and the buried fault, justify the 2-D approximation; however, the magnetization intensities that we derive are likely to be higher than those derived using a 3-D model. The results suggest that the observed anomaly field can be modeled as the effect of a magnetic contrast created by disruption of a magnetized layer whose magnetization is coeval with the highlands crust. The lateral position and width of the inferred gaps in the layer depends on the field inclination.

[44] A range of models was calculated to examine the sensitivity of the results to the field inclination and location and thickness of magnetized blocks. The paleofield inclination was varied from −90° to 90°; results are shown for −60°, −30°, 0° and 30° in Figure 10. Inclinations near zero produce a poor fit to the high-amplitude anomaly north of the buried fault for simple block geometries, while all other models produce an acceptable fit. The models with negative inclination (Figures 10a and 10c) require simpler source geometries to match the observed profile. The depth to the tops of the blocks increases from south to north, mimicking the topography, while the thickness of the blocks varies from a few km to ~15 km on average. The four models in Figure 10 show a range of thickness/intensity values, from a thin layer model (Figure 10a) with high intensity (20 A/m) to a thick layer (up to 19 km) with an intensity of 6 A/m (Figure 10c). A single polarity of magnetization was assumed, however blocks with opposing polarities could also be used within the gaps in the source layer, which would halve the magnetization intensity needed. A significant change in the paleolatitude with time due either to polar wander or tectonic motion during the epoch in which the internal magnetic field was present would result in a variation of paleoinclination for sources magnetized at different epochs. This potential complication is not considered here. The magnetization intensities and layer thicknesses derived in these models is lower by a factor of 3 to 10 relative to the 20 A/m in a 30 km thick layer derived by *Connerney et al.* [1999] for the southern highlands in Terra Cimmeria and Sirenum.

[45] The isostatic anomalies seen in profile in Figure 8 have a similar width and amplitude to the magnetic anomalies, but are displaced to the north. If we assume that

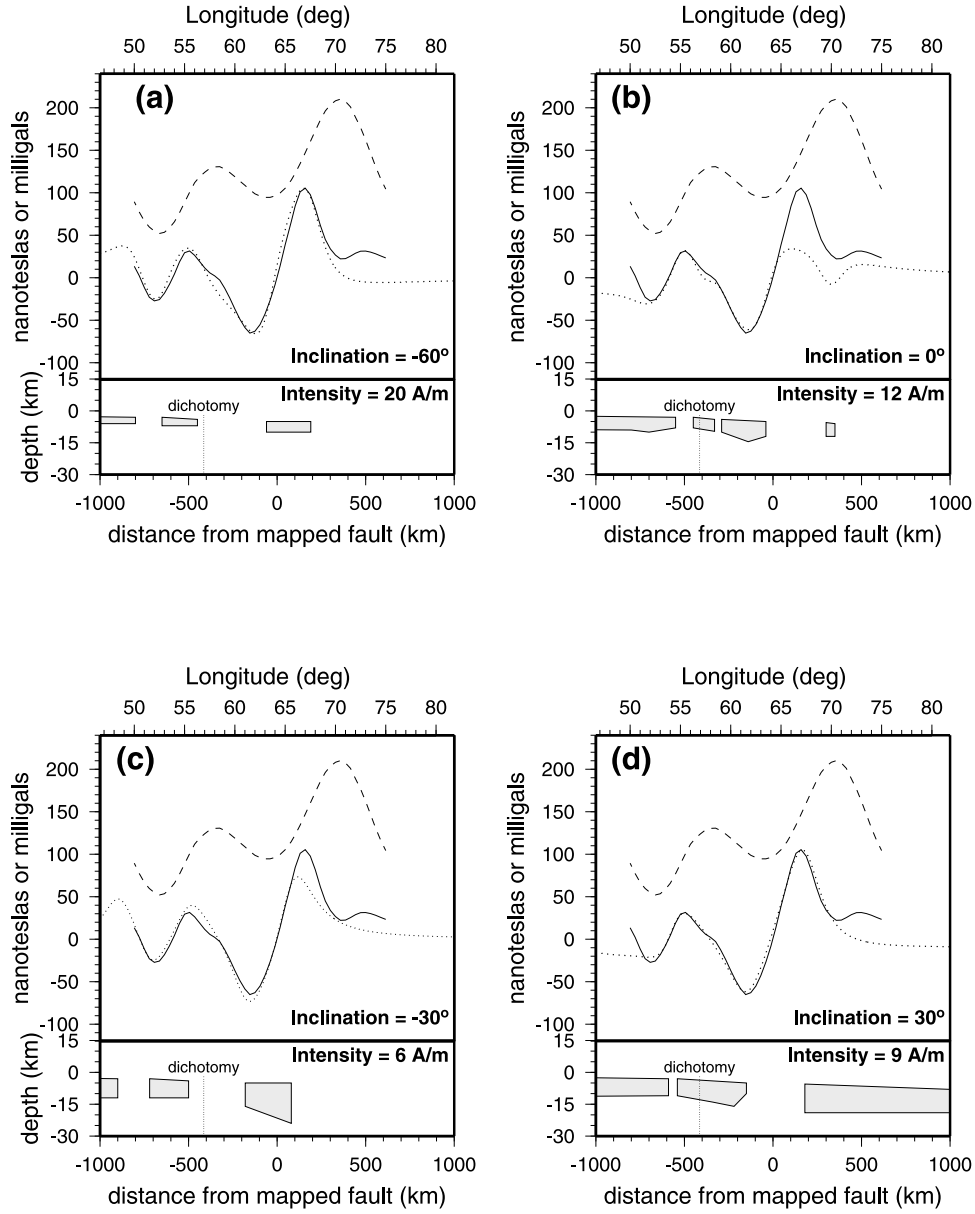

Figure 10. Variations in the dimensions of magnetic source layers for four models with different field inclinations are shown along with the model fits to the observed magnetic field. The source blocks are shown at the bottom of each panel as a function of distance from the buried fault and depth below the highlands topography shown in Figures 1 and 6. The solid line indicates the observed field in nT along a profile perpendicular to the buried fault (Figures 1 and 6), starting in the highlands on the left, crossing the buried fault in the center, and continuing out into the plains. The end points of the profile are 50E, 33N and 75E, 49.5N. The dotted line is the predicted magnetic field in nT. The dashed line is the isostatic gravity profile in milligals. Intensity of magnetization and field inclination assumed for each model are indicated in the figure.

this is due to common sources for the isostatic and magnetic anomalies, rather than a coincidence, then our preferred models are those that result in alignment between the isostatic anomalies and either the magnetized blocks or gaps in the blocks. An inclination of 30° causes the locations of the inferred magnetized bodies to move ~200 km northeast of the observed anomaly peaks, resulting in the best alignment of the blocks of magnetized crust and the location of the positive isostatic anomalies (Figure 9d). This model assumes a magnetization intensity of 9 A/m and the thickness of the magnetized blocks varies from approximately 10 km under the highlands to 12–14 km under the bench, and is greatest (14–15 km) north of the buried fault in the plains. A significant feature of this model is the need for a continuous layer extending into the northern plains to avoid a very high-amplitude negative edge-effect anomaly northeast of the strong positive anomaly north of the fault. This northernmost layer in the model results in a zero net magnetic anomaly in the plains away from the strong positive anomaly, consistent with the observed pattern. The

source regions included in the magnetic models that lie within the northern plains may represent magnetized remnants of Early Noachian crust, similar to the highlands. Alternatively, the −30° inclination model (Figure 10c) has gaps in the magnetized material in the same locations as the isostatic anomalies This model uses a magnetization intensity of 6 A/m, requires less magnetic material to fit the observed field than the 30° inclination model, and does not require a source layer extending into the northern plains. The northern source block ends near the buried fault, and as in the 30° inclination model, there is no contrast between the region just north of the fault and the rest of the plains.

[46] As previously mentioned, an inclination of 0° (Figure 10b) provides a poor fit to the large positive peak north of the fault. No combination of simple blocks can reproduce the observations for very shallow inclinations. A good fit of the model to observed field is obtained for an inclination of −60°, but the locations of the sources for this model do not line up with the locations of the gravity anomalies or the structural patterns. One of the source blocks straddles the buried fault location, and there is no contrast between the region just north of the fault and the rest of the plains. Also, this inclination is outside the limits of the predicted paleofield inclinations discussed previously.

[47] Gaps in the magnetized source layer are required to match the peaks in the magnetic anomalies for all the models we considered. Recognizing the inherent non-uniqueness of magnetic models, any thickness of homogeneously magnetized material of opposite polarity and constant thickness could be included (''annihilator''), within the limits of the observed planetary magnetic moment. Breaks are indicated north and south of the dichotomy boundary, which are required regardless of the assumed inclination of the magnetic field, but which shift in position relative to the structural features as the inclination is varied.

5. Discussion

5.1. Evolution of the Dichotomy

[48] A fundamental question on the evolution of the dichotomy is whether the grabens, scarps, and lowland bench were caused by the original process that formed the dichotomy or if they are a result of subsequent modification. As discussed above, none of the endogenic models for dichotomy formation (except plate tectonics) predict a steep scarp at the boundary, rather a more gradual change in topography would be expected. Yet relatively steep scarps do exist locally, such as the ∼20° scarp in the Ismenius region, and have persisted for billions of years. Specifically, analysis of the stratigraphy and crater counts on the lowland bench and adjacent plateau indicate that the faulting occurred sometime between 3.9 and 3.1 Ga. Although formation of the scarp by primary processes cannot be ruled out, it is likely that the boundary has undergone subsequent modification. If the first stage of the formation of the dichotomy was the creation of different crustal thicknesses between the highlands and lowlands, whether by differentiation or convective processes, then isostatic equilibrium likely occurred quite rapidly, perhaps within 1 my [*Nimmo and Stevenson*, 2001]. Isostatic adjustment alone would result in vertical displacement of the crust rather than extension. If the rheology is strong enough, gravitational relaxation of the highlands topography will take place much more slowly. In regions that have experienced relaxation, the strain at the surface is likely to be small as most strain is accommodated in the weak lower crust [e.g., *Smrekar and Solomon*, 1992]. The observed pattern of faulting is consistent with relaxation of plateau topography. Relaxation models predict extensional faulting at the margin of the plateau, and, for large values of crustal thickness, compression at some distance into the plains. Although the origin of the ridges seen in the topography (Figure 1) is uncertain, their location and orientation is consistent with relaxation of the plateau [*Smrekar and Solomon*, 1992]. If relaxation has taken place, the plateau would have been higher originally. A follow-on study will use the specific relief, pattern of faulting, and formation time of the extension in this region to constrain models of gravitation relaxation of the plateau boundary. These models will be used to estimate the original plateau height, crustal thickness, and thermal history with the goal of discriminating between models of origin.

5.2. Implications of Density and Magnetization Variations

[49] The depth of magnetization of the Martian crust is not well constrained. *Nimmo and Gilmore* [2001] examined the average decrease in magnetization over large impact craters, assuming that large craters would have disrupted the crustal magnetization. For a uniformly magnetized crust, they estimate 35 km as an average depth of magnetization, with bounds of 10–100 km. *Voorhies et al.* [2002] estimate an average depth of ∼46 km based on analysis of the power spectrum of the Martian magnetic field. Other studies have assumed a lower bound on the depth of magnetization based on estimates of the depth to the Curie isotherm at the time of magnetization. This depth is not well known, as there are many possible models for the early thermal evolution of Mars [cf. *Schubert and Spohn*, 1990; *Choblet and Sotin*, 2001; *Breuer and Spohn*, 2003; *Arkani-Hamed*, 2003; and references therein]. Studies of the crustal magnetization have assumed depths of 30–50 km [*Connerney et al.*, 1999; *Arkani-Hamed*, 2002b].

[50] The highland plateau is generally isostatically compensated, as seen in other studies [*Nimmo and Stevenson*, 2001; *McGovern et al.*, 2002; *McKenzie et al.*, 2002; *Nimmo*, 2002]. Our modeling of the admittance in this region also finds that there is little or no flexural compensation (Figure 9). The local crustal thickness is not well constrained, but the global average value of 50 km provides a reasonable fit to the gravity and topography data in this area (see Figure 7a). The Bouguer gravity data (Figure 6d) implies that the lowland bench has thicker crust than the plains but thinner crust than the highlands, such as might occur under a fault block that slipped downward relative to the plateau. To the north of the buried fault there is a further decrease in the crustal thickness. One factor that controls the magnitude of the anomalies is the assumed crustal density for calculation of the Bouguer gravity. If the near-surface density is lower (higher) than the assumed value of 2900 kg/m^3, the amplitude of the Bouguer gravity anomalies will be increased (decreased). For areas covered in sediments, a somewhat lower density is quite plausible. The significant isostatic anomalies, which occur regardless of the crustal thickness, clearly indicate that once contribu-

tions from the topography and crust are removed, there are positive density anomalies under the lowland bench and in the plains northwest and southeast of the buried fault (Figure 7a). These anomalies could be caused by relatively thin intracrustal blocks with excess density (300 kg/m^3 for a 10 km thick layer), or by thicker blocks with a smaller density contrast (100 kg/m^3 for a 30 km thick layer). Alternatively, the anomalies could represent variations in the thickness of the entire crustal layer (see Figure 7b).

[51] The combined geologic and geophysical data suggest post-formation extension and intrusive activity at the boundary possibly accompanied by hydrothermal alteration in broad zones. Faulting, accompanied by subsequent hydrothermal circulation or low-temperature alteration, could have erased the original magnetization, resulting in gaps. The magnetization could also have been lost by heating accompanying intrusions, sub-crustal erosion, or a combination of all of these factors. The correspondence between the magnetic anomalies and the geologic evidence for faulting suggests structural disruption of the source layer as one of the causes of the anomaly pattern in the study area. The width of the inferred break in the source layer surrounding the buried fault argues for a zone of disruption hundreds of kilometers wide, as might be expected due to hydrothermal circulation in a broad zone, rather than the mechanical disruption associated with the fault. Circulation of hydrothermal fluids within a brecciated zone associated with faulting could have demagnetized the material via heating or by altering the magnetic phases after the magnetic field had died off. It is also possible that the gaps in the source layer represent regions of the crust that possess magnetism of reversed polarity, requiring the dynamo to be active and reversing during the evolution of the crust.

[52] Alternatively, the isolated blocks or gaps that correspond to the gravity anomalies in Figure 10 could be intrusions of magma that cooled and became magnetized (Figure 10d), or for which the heating destroyed the magnetization (Figure 10c). The correlation of the magnetic source blocks of the 30° model to the high-density crust indicated by the isostatic gravity data argue for discrete intrusions that were emplaced into the preexisting magnetized crust. For this model, the preexisting magnetized crust exists in the highlands, and persists under the plains. Near the buried fault the plains layer is replaced by a later intrusion of higher density material. For the 30° model, the gaps would then represent areas that have been demagnetized by alteration as discussed above. For the −30° inclination model, the density anomalies would correspond to intrusions that demagnetized the crust, or remagnetized it in an opposite polarity.

5.3. Magmatic Intrusions

[53] The large positive gravity anomalies may indicate the presence of high-density, subsurface intrusions. Although there is no surface manifestation of volcanism, it is possible that either a high-density intrusion formed without any associated surface flows, or that any such flows have been buried by later plains fill material. Analysis of gravity and topography data for a number of large volcanoes indicates that they are constructed from high-density material, ranging from 3000–3150 kg/m^3 [*Arkani-Hamed*, 2000; *McGovern et al.*, 2002; *McKenzie et al.*, 2002]. *Kiefer* [2003, 2004] examined the gravity data for Syrtis Major, Tyrrhena Patera, and Hadriaca Patera. He models the extinct magma chambers using densities of 3300 to 3600 kg/m^3, pointing out that such densities are found for pyroxene and olivine-dominated cumulates, respectively, in Martian meteorites [*Consolmagno and Britt*, 1998; *Britt and Consolmagno*, 2003]. If the high-density material is iron rich, it might also contain greater amounts of magnetic materials.

[54] *King and Anderson* [1995, 1998] proposed that on Earth mantle upwellings could be generated by mantle flow at the transition between thin oceanic lithosphere and thick continental lithosphere. If such a process occurred along the transition between the highlands and lowlands, it could explain the concentration of magnetic anomalies in the plains along the dichotomy boundary as a result of intrusive activity focused near the boundary. As discussed previously, such igneous intrusions could have created new magnetized crust or destroyed magnetized crust by displacement and heating. Considering the high densities inferred for magmas at several late Noachian-early Hesperian volcanoes as discussed above, the correlations between the magnetic sources or gaps and the isostatic anomalies argues for high-density intrusions into the preexisting crust as the cause of the anomalies. However, the emplacement of intrusions would have occurred before the magnetic field shut down in the 30° inclination model, and after the field shut down in the −30° inclination model. The timing of the extension and possible intrusion at the dichotomy boundary can therefore shed light on the timing of the demise of the magnetic field if the paleofield inclination is well determined.

5.4. Hydrothermal Alteration

[55] The other possible explanation for the location of the magnetized crust is that there was once a coherently magnetized layer that experienced localized demagnetization due to mechanical disruption, hydrothermal circulation, or a combination of these factors. The shapes of the faults with depth are unknown, and we can only estimate a lower bound on the fault vertical displacement of 1 km for the buried fault and 2.5 km at the dichotomy boundary scarp, but these displacements could be larger. The depth of hydrothermal circulation on Mars is estimated to be 5–10 km [*Clifford*, 1993], although recent work suggests that hydrothermal circulation could extend much deeper, perhaps down to depths of 20–30 km [*Hanna and Phillips*, 2003; *Solomon et al.*, 2003]. As mechanical disruption due to faulting is likely to be confined to a narrow zone at depth, hydrothermal circulation is likely to be a more significant factor at depth. The zone of disruption and circulation could be due to multiple faults near both the buried fault and at the dichotomy boundary. There is some suggestion that the magnetic field locally correlates with the surface topography. The long-wavelength topography (Figures 6a and 6b) appears to wrap around the magnetic anomalies on either side of the buried fault. The topography in the plains (Figures 1, 6a, and 6b) is highest in the area where the magnetic anomalies are largest (Figure 6). This suggests that the magnetized material is at or within several hundred meters of the surface. Pervasive hydrothermal alteration in the vicinity of the lowland bench and buried fault may have resulted in serpentinization of the crust, which would lower

the bulk density, and cause local uplift. Lower density in the fault zones is consistent with the 30° inclination model but not the −30° inclination model, so for the hypothesis of demagnetization by alteration, the 30° inclination model appears more realistic. The −30° inclination model does not require alteration to disrupt the source layer.

5.4.1. Plains Versus Highlands Magnetism

[56] In each of the models presented in Figure 10 the intensity and direction of magnetization is uniform in each of the magnetic source blocks, extending the highlands magnetized layer into the plains as a disrupted, coherently magnetized layer. These assumptions were chosen to simplify the modeling. The solutions are not unique, nor are they fully realistic given the possible 20° variation in paleofield inclination across the profile studied. However, if paleofield inclination does vary across the study region, as would be expected if the *Arkani-Hamed* [2001] pole is correct, the position of the sources would shift slightly but the solutions would remain valid. The solutions obtained indicate that it is possible to fit the observations with magnetized regions distributed in both the highlands and in the plains. The solution with a field inclination of 30° requires a magnetized layer under the plains north of the buried fault, which would be barely detectable at MGS altitudes, and which would contribute little to the total planetary magnetic moment. Weak magnetization of the plains, except within the impact basins, is thus permissible and required for this choice of model assumptions. Alternatively, for the model with a magnetic field inclination of −30°, the surviving magnetized crust is limited to roughly the edge of the lowland bench, interpreted as the extent of the down-faulted highlands crust. This model suggests that all the magnetic anomalies in the plains near the dichotomy boundary could result from material originally part of the highlands. Distinguishing between these interpretations would have important implications for the timing and history of plains magnetization. Further work on the three dimensional structure of subsurface magnetized blocks along the dichotomy may make it possible to determine which hypothesis is most likely.

6. Conclusions

[57] The region between 50 and 90E contains the least modified section of the dichotomy boundary. A relatively steep boundary scarp and grabens characterize the area. Stratigraphic relationships, topography, and crater ages indicate that a section of the highlands was down faulted to the north, creating a lowland bench of highland crust. The northern edge of this bench is defined by an abrupt decrease in topographic knobs, and was mapped by *Dimitriou* [1990] as a buried fault. Strain estimates indicate a lower bound on extension of 3.5% across the dichotomy boundary. The scarps in this region could not have been a primary result of erosion. The basement age of the lowland bench is similar to the basement age of the highland plateau. Given their early Noachian age, a large scarp could not have formed prior to this time and survived the heavy bombardment. With the exception of plate tectonics, which is unlikely for other reasons, none of the proposed models for the formation of the dichotomy predict an initially steep scarp. We thus infer that the observed scarps and extension across the boundary are a result of subsequent modification. The location of faulting and the amount of strain are broadly consistent with gravitational relaxation. More detailed models of this process will be applied to this area in the future to determine if this process is viable, and to assess rheological implications [*Guest and Smrekar*, 2004]. Magmatic intrusions at depth (as discussed above) may be related to the extension.

[58] Modeling of the gravity and topography in this area indicates that the region is isostatically compensated, as is typical of the highlands [*McGovern et al.*, 2002; *McKenzie et al.*, 2002; *Nimmo*, 2002]. The crust in this area is thickest under the highlands and thinnest under the plains, and intermediate in thickness under the lowland bench. Large density variations in the plains appear to have a variety of origins. Some are associated with features that extend beyond the study area, such as the Utopia basin and a large gravity high in the northern plains. The isostatic anomaly indicates the presence of high-density material to the south and north of the buried fault. These areas may indicate subsurface intrusions. Analysis of gravity data for a number of large volcanoes on Mars indicates that they consist of rocks with considerably higher density than normal crust [*Arkani-Hamed*, 2000; *Kiefer*, 2003, 2004; *McGovern et al.*, 2002; *McKenzie et al.*, 2002]. Such intrusions may be localized along the dichotomy boundary due to a difference in lithospheric thickness, as proposed for the Earth [*King and Anderson*, 1995, 1998].

[59] Models of a magnetic field profile across the highland plateau, lowland bench, buried fault, and plains illustrate possible distributions of magnetic sources, obtained using a single intensity and magnetization direction for each model, but varying the source dimensions. Paleofield inclinations for this area are estimated to be in the range ∼−20 to 60° [*Arkani-Hamed*, 2001; *Hood and Zakharian*, 2001]. Models with inclinations of +30° and −30° result in correlated locations for the sources of the magnetic and gravity anomalies. The −30° inclination model has gaps in the magnetization (relative to the highlands source layer) that are approximately aligned with the isostatic gravity anomalies. These gaps are consistent with discrete high-density intrusions causing demagnetization of the crust. For this solution, the magnetization of the crust only extends to the approximate location of the buried fault. If this model is correct, it suggests that the tendency of the magnetic anomalies to follow the dichotomy boundary may be caused by blocks of down-faulted highlands crust resting at the plains elevation. The alternate model with a field inclination of 30° has blocks of magnetized crust rather than gaps aligned with the isostatic gravity anomalies, as well as magnetization extending into the plains. In this model, a magnetized intracrustal layer with a thickness of ∼10 km, an intensity of 9 A/m, and an excess density of 150 kg/m^3 provide a good fit to the data. Gaps in the magnetized crust for the 30° inclination model could result from hydrothermal alteration of the crust in a distributed zone on either side of the buried fault. Within this interpretation of the magnetic field, the excess density required by the isostatic anomalies could be a result of intrusions, thinning of the crust, differences in the composition, or a decrease in the density near the fault zones due to serpentinization. Further modeling of

the three dimensional structure of the crust here and along other areas of the dichotomy boundary may make it possible to distinguish between these possibilities.

[60] **Acknowledgments.** This work was supported by a NASA grant from the Mars Data Analysis Program. We thank Susan Sakimoto and Tom Watters for their reviews, which helped to improve this paper.

References

Acuna, M. H., et al. (1999), Global distribution of crustal magnetization discovered by the Mars Global Surveyor MAG/ER experiment, *Science*, *284*, 700–793.

Acuna, M. H., et al. (2001), Magnetic field of Mars: Summary of results from the aerobraking and mapping orbits, *J. Geophys. Res.*, *106*(E10), 23,403–23,417.

Arkani-Hamed, J. (2000), Strength of the Martian lithosphere beneath large volcanoes, *J. Geophys. Res.*, *105*(E11), 26,712–26,732.

Arkani-Hamed, J. (2001), Paleomagnetic pole positions and pole reversals of Mars, *Geophys. Res. Lett.*, *28*, 3409–3412.

Arkani-Hamed, J. (2002a), An improved 50-degree spherical harmonic model of the magnetic field of Mars derived from both high-altitude and low-altitude data, *J. Geophys. Res.*, *107*(E10), 5083, doi:10.1029/2001JE001835.

Arkani-Hamed, J. (2002b), Magnetization of the Martian crust, *J. Geophys. Res.*, *107*(E5), 5032, doi:10.1029/2001JE001496.

Arkani-Hamed, J. (2003), Thermoremanent magnetization of the Martian lithosphere, *J. Geophys. Res.*, *108*(E10), 5114, doi:10.1029/2003JE002049.

Breuer, D., and T. Spohn (2003), Early plate tectonics versus single-plate tectonics on Mars: Evidence from magnetic field history and crust evolution, *J. Geophys. Res.*, *108*(E7), 5072, doi:10.1029/2002JE001999.

Breuer, D., T. Spohn, and U. Wuller (1993), Mantle differentiation and the crustal dichotomy of Mars, *Planet. Space Sci.*, *41*, 269–283.

Breuer, D., D. A. Yuen, and T. Spohn (1997), Phase transitions in the Martian mantle: Implications for partially layered convection, *Earth Planet. Sci. Lett.*, *148*, 457–469.

Breuer, D., D. A. Yuen, T. Spohn, and S. Zhang (1998), Three-dimensional models of Martian mantle convection with phase transitions, *Geophys. Res. Lett.*, *25*, 229–232.

Britt, D. T., and G. J. Consolmagno (2003), Stony meteorite porosities and densities: A review of the data through 2001, *Meteorit. Planet. Sci.*, *38*(8), 1161–1180.

Cain, J. C., B. B. Ferguson, and D. Mozzoni (2003), An $n = 90$ internal potential function of the Martian crustal magnetic field, *J. Geophys. Res.*, *108*(E2), 5008, doi:10.1029/2000JE001487.

Carruthers, M. W., and G. E. McGill (1998), Evidence for igneous activity and implications for the origin of a fretted channel in southern Ismenius Lacus, Mars, *J. Geophys. Res.*, *103*, 31,433–31,443.

Chen, J. H., and G. J. Wasserburg (1986), Formation ages and evolution of shergotty and its parent planet from U-Th-Pb systematics, *Geochim. Cosmochim. Acta*, *50*, 955–968.

Choblet, G., and C. Sotin (2001), Early transient cooling of Mars, *Geophys. Res. Lett.*, *28*(15), 2035–3038.

Clifford, S. M. (1993), A model for the hydrologic and climate behavior of water on Mars, *J. Geophys. Res.*, *98*, 10,973–111,016.

Connerney, J., M. H. Acuña, P. Wasilewski, N. F. Ness, H. Rème, C. Mazelle, D. Vignes, R. P. Lin, D. Mitchell, and P. Cloutier (1999), Magnetic lineations in the ancient crust of Mars, *Science*, *284*, 794–798.

Connerney, J., M. Acuña, P. Wasilewski, G. Kletetschka, N. Ness, H. Rème, R. Lin, and D. Mitchell (2001), The global magnetic field of Mars and implications for crustal evolution, *Geophys. Res. Lett.*, *28*(21), 4015–4018.

Consolmagno, G. J., and D. T. Britt (1998), The density and porosity of meteorites from the Vatican collection, *Meteorit. Planet. Sci.*, *33*(6), 1231–1241.

Craddock, R. A., and T. A. Maxwell (1993), Geomorphic evolution of the Martian highlands through ancient fluvial processes, *J. Geophys. Res.*, *98*, 3453–3468.

Dimitriou, A. M. (1990), Clues to an upland/lowland boundary forming event: The stratigraphy and topography of the Ismenius Lacus SE subquadrangle, Mars., M.S. thesis, Univ. of Mass., Amherst.

Edgett, K. S., and T. J. Parker (1997), Water on early Mars: Possible subaqueous sedimentary deposits covering ancient cratered terrain in western Arabia and Sinus Meridiani, *Geophys. Res. Lett.*, *24*, 2897–2900.

Frey, H. V. (2004), A timescale for major event in early Mars crustal evolution, *Lunar Planet. Sci.* [CD-ROM], *XXXIV*, abstract 1382.

Frey, H., and R. A. Schultz (1988), Large impact basins and the mega-impact origin for the crustal dichotomy, *Geophys. Res. Lett.*, *15*, 229–232.

Frey, H., A. M. Semeniuk, J. A. Semeniuk, and S. Tokarcik (1988), A widespread common age resurfacing event in the highland-lowland transition zone in eastern Mars, *Proc. Lunar Planet. Sci. Conf. 18th*, 679–699.

Frey, H., S. E. Sakimoto, and J. Roark (1998), The MOLA topographic signature at the crustal dichotomy boundary zone on Mars, *Geophys. Res. Lett.*, *25*, 4409–4412.

Frey, H. V., J. H. Roark, K. M. Shockey, E. L. Frey, and S. E. H. Sakimoto (2002), Ancient lowlands on Mars, *Geophys. Res. Lett.*, *29*(10), 1384, doi:10.1029/2001GL013832.

Garvin, J. B., S. E. H. Sakimoto, and J. J. Frawley (2003), Craters on Mars: Geometric properties from gridded MOLA topography, in 6th International Conference on Mars, abstract 3277, Lunar and Planet. Inst., Houston, Tex.

Grant, J. A., and P. H. Schultz (1990), Gradational epochs on Mars: Evidence from west-northwest of Isidis basin and Electris, *Icarus*, *84*, 166–195.

Greeley, R., and J. E. Guest (1987), Geologic map of the eastern equatorial region of Mars, *U.S. Geol. Surv. Misc. Invest. Ser., Map I-1802-B*.

Guest, A., and S. E. Smrekar (2004), Relaxation of the Martian crustal dichotomy boundary in the Ismenius region, *Lunar Planet. Sci.* [CD-ROM], *XXXIV*, abstract 1362.

Hanna, J. C., and R. J. Phillips (2003), A new model of the hydrologic properties of the Martian crust and implications for the formation of valley networks and outflow channels, *Lunar Planet. Sci.* [CD-ROM], *XXXIII*, abstract 2027.

Hartmann, W. K., and G. Neukum (2001), Cratering chronology and the evolution of Mars, in *Chronology and Evolution of Mars*, edited by R. Kallenback, J. Geiss, and W. K. Hartmann, pp. 165–194, Kluwer Acad., Norwell, Mass.

Hiller, K. H. (1979), Geologic map of the Amenthes quadrangle, Mars, *U.S. Geol. Surv. Misc. Invest. Ser., Map I-1110*.

Hood, L. L., and A. Zakharian (2001), Mapping and modeling of magnetic anomalies in the northern polar region of Mars, *J. Geophys. Res.*, *106*, 14,601–14,619.

Hynek, B. M., and R. J. Phillips (2001), Evidence for extensive denudation of the Martian highlands, *Geology*, *29*, 407–410.

Kiefer, W. S. (2004), Gravity evidence for an extinct magma chamber beneath Syrtis Major, Mars: A look at the magmatic plumbing system, *Earth Planet. Sci. Lett.*, *222*, 349–361.

Kiefer, W. S. (2003), Gravity evidence for extinct magma chambers on Mars: Tyrrhena Patera and Hadriaca Patera, *Lunar Planet. Sci.* [CD-ROM], *XXXIII*, abstract 1234.

King, S. D., and D. L. Anderson (1995), An alternative mechanism of flood basalt formation, *Earth Planet. Sci. Lett.*, *136*, 269–279.

King, S. D., and D. L. Anderson (1998), Edge-driven convection, *Earth Planet. Sci. Lett.*, *160*, 289–296.

Kochel, R. C., and R. T. Peake (1984), Quantification of waste morphology in Martian fretted terrain, *Proc. Lunar Planet. Sci. Conf. 15th*, Part 1, *J. Geophys. Res.*, *89*, suppl., C336–C350.

Lenardic, A., F. Nimmo, and L. Moresi (2004), Growth of the hemispheric dichotomy and the cessation of plate tectonics on Mars, *J. Geophys. Res.*, *109*, E02003, doi:10.1029/2003JE002172.

Lucchitta, B. K. (1978), Geologic map of the Ismenius Lacus region of Mars, *U.S. Geol. Surv. Misc. Invest. Ser., Map I-1065*.

Maxwell, T. A., and G. E. McGill (1988), Ages of fracturing and resurfacing in the Amenthes region, Mars, *Proc. Lunar Planet. Sci. Conf. 18th*, 701–711.

McGill, G. E. (1989), Buried topography of Utopia, Mars: Persistence of a giant impact depression, *J. Geophys. Res.*, *94*, 2753–2759.

McGill, G. E. (2000), Crustal history of north central Arabia Terra, Mars, *J. Geophys. Res.*, *105*, 6945–6959.

McGill, G. E. (2002), Geologic map transecting the highland/lowland boundary zone, Arabia Terra, Mars: Quadrangles 30332, 35332, 40332, and 45332, *U.S. Geol. Surv. Geol. Invest. Ser., Map I-2746*.

McGill, G. E., and A. M. Dimitriou (1990), Origin of the Martian global dichotomy by crustal thinning in the late Noachian or early Hesperian, *J. Geophys. Res.*, *95*, 12,595–12,605.

McGill, G. E., and S. W. Squyres (1991), Origin of the Martian crustal dichotomy: Evaluating hypotheses, *Icarus*, *93*, 386–393.

McGovern, P. J., S. C. Solomon, D. E. Smith, M. T. Zuber, M. Simons, M. A. Wieczorek, R. J. Phillips, G. A. Neumann, O. Aharonson, and J. W. Head (2002), Localized gravity/topography admittance and correlation spectra on Mars: Implications for regional and global evolution, *J. Geophys. Res.*, *107*(E12), 5136, doi:10.1029/2002JE001854.

McKenzie, D., D. N. Barnett, and D. Yuan (2002), The relationship between Martian gravity and topography, *Earth Planet. Sci. Lett.*, *195*, 1–16.

Moore, J. M. (1990), Nature of the mantling deposit in the heavily cratered terrain of northeastern Arabia, Mars, *J. Geophys. Res.*, *95*, 14,279–14,289.

Mutch, T. A., R. E. Arvidson, J. W. Head III, K. L. Jones, and R. S. Saunders (1976), *The Geology of Mars*, Princeton Univ. Press, Princeton, N. J.

Neukum, G., and K. Hiller (1981), Martian ages, *J. Geophys. Res.*, *86*, 3097–3121.

Nimmo, F. (2002), Admittance estimates of mean crustal thickness and density at the Martian hemispheric dichotomy, *J. Geophys. Res.*, *107*(E11), 5117, doi:10.1029/2000JE001488.

Nimmo, F., and M. S. Gilmore (2001), Constraints on the depth of magnetized crust on Mars from impact craters, *J. Geophys. Res.*, *106*(E6), 12,315–12,323.

Nimmo, F., and D. J. Stevenson (2001), Estimates of Martian crustal thickness from viscous relaxation of topography, *J. Geophys. Res.*, *106*(E3), 5085–5098.

Parker, T. J., R. S. Saunders, and D. M. Schneeberger (1989), Transitional morphology in west Deuteronilus Mensae, Mars: Implications for modification of the lowland/upland boundary, *Icarus*, *82*, 111–145.

Phillips, R. J., M. T. Zuber, S. C. Solomon, M. P. Golombek, B. M. Jakosky, W. B. Banerdt, R. M. E. Williams, B. M. Hynek, O. Aharonson, and S. A. Hauck II (2001), Ancient geodynamics and global-scale hydrology on Mars, *Science*, *291*, 2587–2591.

Pike, R. J., and P. A. Davis (1984), Toward a topographic model of Martian craters from photoclinometry, *Lunar Planet. Sci.*, *XV*, 645–646.

Purucker, M., D. Ravat, H. Frey, C. Voorhies, T. Sabaka, and M. Acuna (2000), An altitude-normalized magnetic map of Mars and its interpretation, *Geophys. Res. Lett.*, *27*, 2449–2452.

Schubert, G., and T. Spohn (1990), Thermal history of Mars and the sulphur content of its core, *J. Geophys. Res.*, *95*, 14,095–14,101.

Scott, D. H., and K. L. Tanaka (1986), Geological map of the western equatorial region of Mars, *U.S. Geol. Surv. Misc. Invest. Ser., Map I-1802-A*.

Sharp, R. P. (1973), Fretted and chaotic terrain, *J. Geophys. Res.*, *78*, 4073–4083.

Sleep, N. H. (1994), Martian plate tectonics, *J. Geophys. Res.*, *99*, 5639–5655.

Smith, D. E., et al. (1999), The global topography of Mars and implications for surface evolution, *Science*, *284*, 1495–1503.

Smrekar, S. E., and S. C. Solomon (1992), Gravitational spreading of high terrain in Ishtar Terra, Venus, *J. Geophys. Res.*, *97*, 16,121–16,148.

Smrekar, S. E., R. Comstock, and F. S. Anderson (2003), A gravity survey of Type 2 coronae on Venus, *J. Geophys. Res.*, *108*(E8), 5090, doi:10.1029/2002JE001935.

Solomon, S. C., et al. (2003), Why are there so few magnetic anomalies in Martian lowlands and basins?, *Lunar Planet. Sci.* [CD-ROM], *XXXIII*, abstract 1382.

Squyres, S. W. (1979), The distribution of lobate debris aprons and similar flows on Mars, *J. Geophys. Res.*, *84*, 8087–8096.

Stevenson, D. J. (1980), Lunar asymmetry and paleomagnetism, *Nature*, *287*, 520–521.

Tanaka, K. L. (1986), The stratigraphy of Mars, *Proc. Lunar Planet. Sci. Conf. 17th*, Part 1, *J. Geophys. Res.*, *91*, suppl., E139–E158.

Tanaka, K. L. (2000), Dust and ice deposition in the Martian geologic record, *Icarus*, *144*, 254–266.

Tanaka, K. L., D. H. Scott, and R. Greeley (1992), Global stratigraphy, in *Mars*, edited by H. H. Kieffer et al., pp. 345–382, Univ. Ariz. Press, Tucson.

Voorhies, C. V., T. J. Sabaka, and M. Purucker (2002), On magnetic spectra of Earth and Mars, *J. Geophys. Res.*, *107*(E6), 5034, doi:10.1029/2001JE001534.

Watters, T. R. (2003a), Lithospheric flexure and the origin of the dichotomy boundary on Mars, *Geology*, *31*, 271–274.

Watters, T. R. (2003b), Thrust faults along the dichotomy boundary in the eastern hemisphere of Mars, *J. Geophys. Res.*, *108*(E6), 5054, doi:10.1029/2002JE001934.

Wilhelms, D. E., and S. W. Squyres (1984), The Martian hemispheric dichotomy may be due to a giant impact, *Nature*, *309*, 138–140.

Wise, D. U., M. P. Golombek, and G. E. McGill (1979a), Tharsis province of Mars: Geologic sequence, geometry, and a deformation mechanism, *Icarus*, *38*, 456–472.

Wise, D. U., M. P. Golombek, and G. E. McGill (1979b), Tectonic evolution of Mars, *J. Geophys. Res.*, *84*, 7934–7939.

Yuan, D., W. Sjogren, A. Konopliv, and A. Kucinskas (2001), Gravity field of Mars: A 75th Degree and Order Model, *J. Geophys. Res.*, *106*(E10), 23,377–23,402.

Zhong, S., and M. T. Zuber (2001), Degree-1 mantle convection and the crustal dichotomy on Mars, *Earth Planet. Sci. Lett.*, *189*, 75–84.

Zhong, S., E. M. Parmentier, and M. T. Zuber (2000), A dynamic origin for the global asymmetry of lunar mare basalts, *Earth Planet. Sci. Lett.*, *117*, 113–140.

Zuber, M. T. (2001), The crust and mantle of Mars, *Nature*, *412*, 220–227.

Zuber, M. T., D. E. Smith, F. G. Lemoine, and G. A. Neumann (1994), The shape and internal structure of the Moon from the Clementine Mission, *Science*, *266*(5192), 1839–1843.

Zuber, M. T., et al. (2000), Internal structure and early thermal evolution of Mars from Mars Global Surveyor topography and gravity, *Science*, *287*, 1788–1793.

A. M. Dimitriou, SLR Alaska, 2525 Blueberry Road, Suite 206, Anchorage, AK 99503, USA.

G. E. McGill, Department of Geosciences, University of Massachusetts, Amherst, MA 01003, USA.

C. A. Raymond and S. E. Smrekar, Jet Propulsion Laboratory, California Institute of Technology, Mail Stop 183-501, 4800 Oak Grove Drive, Pasadena, CA 91109, USA. (ssmrekar@jpl.nasa.gov)